Cone Penetration Testing 2018 – Hicks, Pisanò & Peuchen (Eds)

Penetrometer equipment and testing techniques for offshore design of foundations, anchors and pipelines

M.F. Randolph, S.A. Stanier, C.D. O'Loughlin, S.H. Chow, B. Bienen, J.P. Doherty, H. Mohr, R. Ragni & M.A. Schneider
University of Western Australia, Perth, Australia

D.J. White
University of Southampton, Southampton, UK

J.A. Schneider
USACE, St. Paul, MN, USA

ABSTRACT: This paper attempts to categorise geotechnical field site characterisation tools in a hierarchical manner, as appropriate for the progression from initial surveys to detailed geotechnical design of specific infrastructure. In general, the hierarchy reflects more the sophistication, and hence cost, of the field tools, although small-scale tools developed to explore box core samples are something of an exception, with the potential for high quality data at low cost. These ideas are explored in the context of modern developments in equipment and methods of deployment, and in the manner in which the data may be used efficiently in design.

1 INTRODUCTION

The current economic climate for offshore energy is requiring improved efficiency in the design of subsea infrastructure, a key starting point for which is optimising site investigation (SI) data and their application in design. Geotechnical design for deep water developments is dominated by subsea infrastructure such as subsea foundation units and in-field pipelines founded within the uppermost sediment layers. Even anchoring systems, particularly for mobile drilling systems, will generally lie within the top 10 to 20 m of the seabed. Hence the vast majority of deep water infrastructure is founded within sediments that are well within reach of relatively modest-sized robotic seabed tools or free-fall penetrometers. There is, however, a marked difference between testing requirements for pipeline design parameters, where the focus is generally the upper 0.5 m of the seabed, and those for subsea foundations and anchors.

For coastal and other shallow water developments, the challenge of acquiring in situ test data is reduced somewhat, although for applications like cable laying it may be sufficient just to identify sediment type. Economic pressures, particularly for wind and wave energy applications, will require optimisation of the spatial frequency of acquiring data in situ, and how the data are then applied in design to best advantage.

This paper discusses advances in site investigation approaches, with initial focus on novel approaches for near-surface characterisation and cost-effective free-fall penetrometry, which have particular relevance for deep water projects or for identifying surficial sediment types generally. The advances are considered in light of the need to balance cost and quality of data at different phases of a project. The paper also discusses the growth in 'direct' use of CPT data in design methods, such as for jack-up rig foundations. Potential differences between 'indirect' use of CPT data to derive simplified strength profiles, and more direct incorporation of what may appear relatively minor fluctuations in the cone resistance through the stratigraphy, are examined.

2 PHASES OF GEOTECHNICAL SITE CHARACTERISATION

2.1 *Exploratory phases*

For a new development, early investigation phases are focused on obtaining geophysical data in order to establish a broad geological model for the region. Historically, very limited (if any) geotechnical data

on the upper seabed sediments are obtained until later. This approach is influenced to a large degree by cost, since geophysical data may be gathered using relatively small vessels, with limited deck space for accommodating geotechnical investigation equipment.

Nowadays, however, lightweight (compact) tools, such as box core samplers, free-fall penetrometers and lightweight seabed frames equipped with small diameter coiled rod cone penetrometers are being incorporated increasingly in geophysical investigations. These provide early indications of the near-surface sediment properties, which are difficult to assess from standard seismic reflection tools (Peuchen & Westgate 2018).

In spite of inevitable disturbance of the soil recovered in a box core, reasonable quantitative estimates of intact and remoulded shear strength may be obtained from miniature penetrometer (T-bar or ball) tests conducted in the upper 0.3 m or so, depending on sample recovery (Low et al. 2008). As discussed in more detail later, additional parameters for pipeline design may be determined from torsional tests on novel types of penetrometer (White et al. 2017).

Free-fall penetrometers also offer cost-effective investigation of the near surface seabed. Even simple devices that just measure the deceleration (e.g. Stark et al. 2009, 2012) will allow approximate estimation of the strength of the upper sediments, providing useful guidance for pipeline route assessment. Modern lightweight free-fall piezocones offer much more quantitative assessment of the strength profiles through the upper material (Stegmann et al. 2006), provided the interpretation approach is appropriate (Chow et al. 2017).

2.2 *Main geotechnical SI phases*

In the main phases of geotechnical site investigation, larger vessels capable of handling larger and more sophisticated drilling and field testing equipment are used. Even here, though, the modern trend is for more compact, seabed-based robotic drilling and testing equipment, rather than conventional drill ships. In deep water, seabed-based systems are preferable in terms of cost (with compact equipment allowing smaller vessels) and datum stability since the systems are decoupled from wave-induced vessel motions.

Advances in robotic control have led to a number of commercial seabed-based robotic drilling, sampling and testing systems. The pioneer amongst these in terms of increased depth of water and soil depth investigated was the portable remotely operated drill (PROD), developed by Benthic Geotech (Figure 1). The equipment fits within standard shipping containers for transport.

Figure 1. Benthic Geotech's portable remotely operated drill (PROD).

Figure 2. Fugro seafloor drill.

PROD and other systems, such as the Fugro Seafloor Drill (Figure 2), use an umbilical cable to power the seabed frame, although smaller systems can use remotely operated vehicles (ROVs) as a power source (Randolph 2016).

Seabed frames with advanced actuation offer the potential for more sophisticated penetration testing, for example by varying the rate of penetration in order to explore effects of strain rate and partial consolidation. This can yield measurements

that are more representative of conditions around the target infrastructure—which may involve significant changes in soil strength due to installation and in-service loading.

Full-flow penetrometers, such as the T-bar and piezoball with projected areas typically a factor of 10 greater than that of the shaft immediately behind the probe, provide potential for cyclic motion in order to remould the surrounding soil. They are often considered as applicable only for shallow uniform fine-grained sediments. However, experience in layered carbonate material has shown that they provide consistent data to CPTs in layered sediments, generally with T-bar and ball resistances showing slightly lower magnitudes of spikes in resistance (see Figure 3).

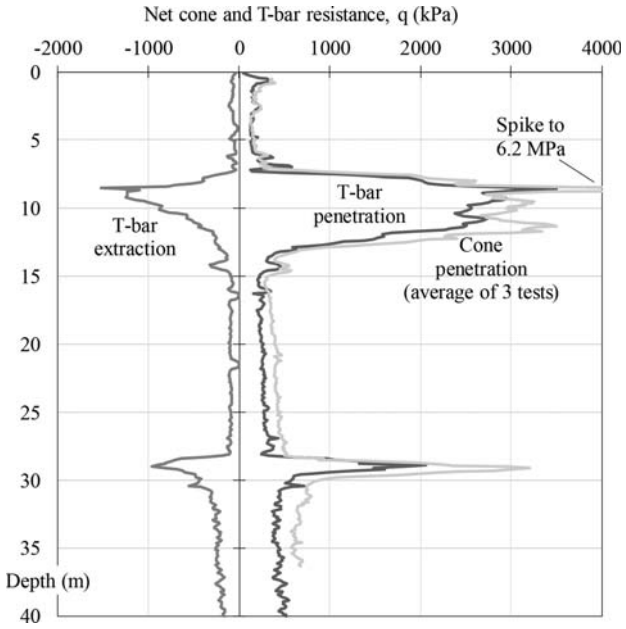

Figure 3. Comparison of in situ cone and T-bar penetration tests from Australian North-West Shelf.

The addition of pore pressure sensors on so-called 'piezoball' penetrometers, either as discrete button filters or continuous annular filters, enhances their potential as a stratification tool, and also allows field assessment of consolidation properties by means of dissipation tests (Mahmoodzadeh et al. 2015).

As illustration of this potential, Figure 4 shows the range of penetration resistance mobilised in a carbonate silt, relative to a standard rate penetration test. The data are from the RIGSS JIP (White et al. 2017) and span a factor of 20 between fully remoulded conditions and those after full consolidation.

The data from Figure 4 were obtained under laboratory conditions, in a centrifuge model test, although similar data may be acquired from in situ tests. In the carbonate silt, penetration under undrained conditions even at the very high rates associated with free-fall penetrometers, gives lower resistance than for drained conditions at a very slow penetration rate. In stronger soils, such as medium dense silica sand, undrained conditions will most likely provide the highest penetration resistance due to the dilative nature of such soils. The effect of sand density on the relative magnitudes of drained and undrained penetration resistances is well illustrated by the penetrometer data presented by Chow et al. (2018).

The very high resistances in sand mobilised under undrained conditions have been observed in field free-fall penetrometer tests, leading to rapid arrest of the penetrometer (Stark et al. 2012). Although this limits the depth that can be

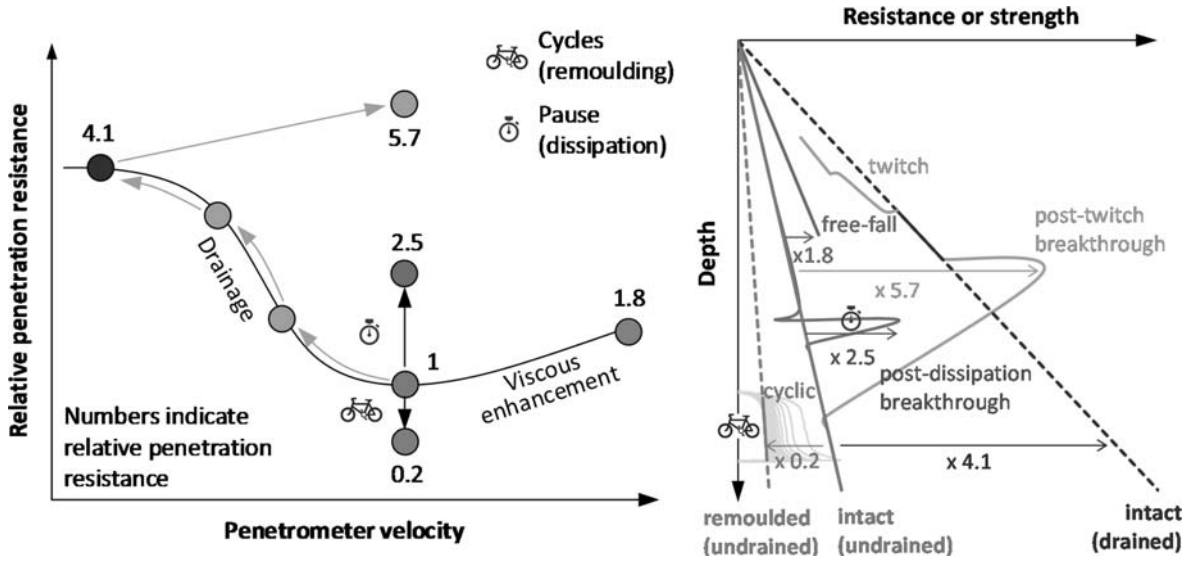

Figure 4. Penetration resistances mobilised in a carbonate silt through different penetrometer test procedures.

explored, the information of shallow sandy sediments with high (undrained) penetration resistance has value for design. With some additional inputs, for example knowledge of mineralogy and particle size of the sediments, the deduced penetration resistances may be interpreted in terms of relative density, in the same way as for static CPTs (White et al. 2018).

Prior to cavitation the undrained strength of sand may be estimated using the framework of Bolton (1986) or a state parameter approach (Been et al. 1991). After cavitation, although this is unlikely to occur in deep water, an upper limit to the penetration resistance may be estimated by considering the cavitation pressure as a 'back pressure' acting in conjunction with the geostatic effective stress state.

Improvements in control and testing procedures open the door to much more sophisticated seabed testing. Figure 5 shows schematically the range of shear strength data that may be acquired, relative to strengths relevant for design of different offshore infrastructure. The diagram reflects the variations in penetration resistance arising from different testing procedures, as discussed with respect to Figure 4. The horizontal spread reflects changes in strength due to consolidation (left side) or disturbance and remoulding (right side), while the vertical axis signifies changes in strength due to shear strain rate.

Modern robotic systems also have the control potential to allow seabed testing that targets stiffness measurement. For example, fatigue design of riser systems requires information on the vertical riser-soil stiffness, and how that varies with time and displacement amplitude of cyclic perturbations.

For a steel catenary riser, the relevant stiffness may vary by 1 or 2 orders of magnitude through the touchdown zone as the displacement amplitude of the riser changes. At a given amplitude, the stiffness will also tend to reduce in the short term as the soil responds to cyclic shearing, but to increase with time due to consolidation (Clukey et al. 2017, Yuan et al. 2017).

Future potential for field tests, either on the seabed or in recovered box core samples (Kelleher et al. 2010, Boscardin & DeGroot 2015), is discussed in the following section, drawing on recent experience on Australia's North-West Shelf and in the Caspian Sea.

3 NOVEL SHALLOW PENETROMETERS FOR PIPELINE DESIGN PARAMETERS

3.1 *Background—RIGSS JIP*

The Remote Intelligent Geotechnical Seabed Surveys Joint Industry Project (RIGSS JIP) was initiated by the University of Western Australia (UWA) and is reaching the end of the 3 year program of activities. A focus of the JIP has been the development of new and improved techniques for in-situ geotechnical investigation of the upper few metres of the seabed.

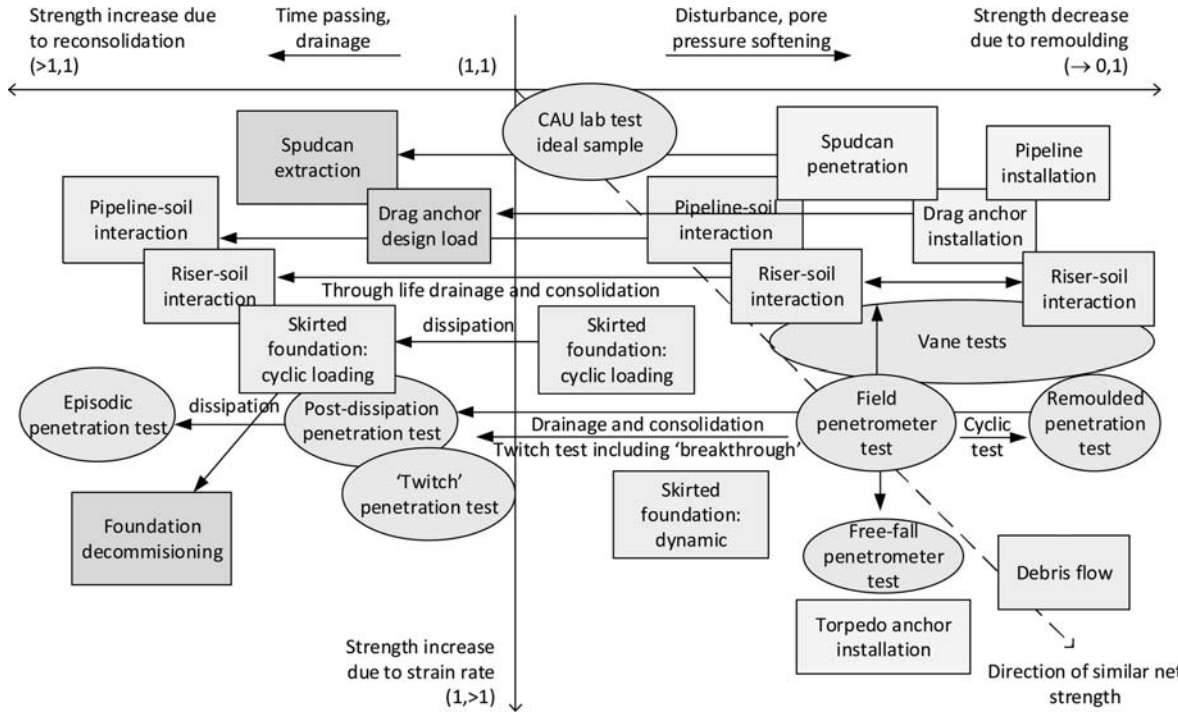

Figure 5. Map of different soil tests and design applications (extended from Randolph et al. 2007).

The RIGSS JIP has pursued three 'visions', which are illustrated in Figure 6:

1. The RIGSS SI: A remote SI platform with robotic control of intelligent tools gathering parameters targeted towards design.
2. Earlier geotechnical definition in projects: leading to reduced uncertainty and risk, and a reduced need to carry multiple options through design.
3. Direct geotechnical design: a design philosophy using in situ test data more directly to determine the response of pipelines, foundations, and other geotechnical systems

Together, these three ideas aim to allow more accurate forecasting of the behaviour of seabed infrastructure. New types of penetrometer can be shaped and manipulated in ways that more closely represent the infrastructure being designed. The resulting data provide the potential to eliminate or simplify the journey from measured resistance to a lab-based strength and back to a predicted resistance or capacity.

A particular focus of the RIGSS JIP has been on shallow surveys that cover extensive areas, such as for pipelines, where low-cost, remotely operated SI tools and smart testing techniques offer potential to improve efficiency and deliver more valuable data. Intelligent tools—such as the shallow penetrometers—give data that can be fed more directly into geotechnical design, reducing the timescale and uncertainty associated with the design outcome.

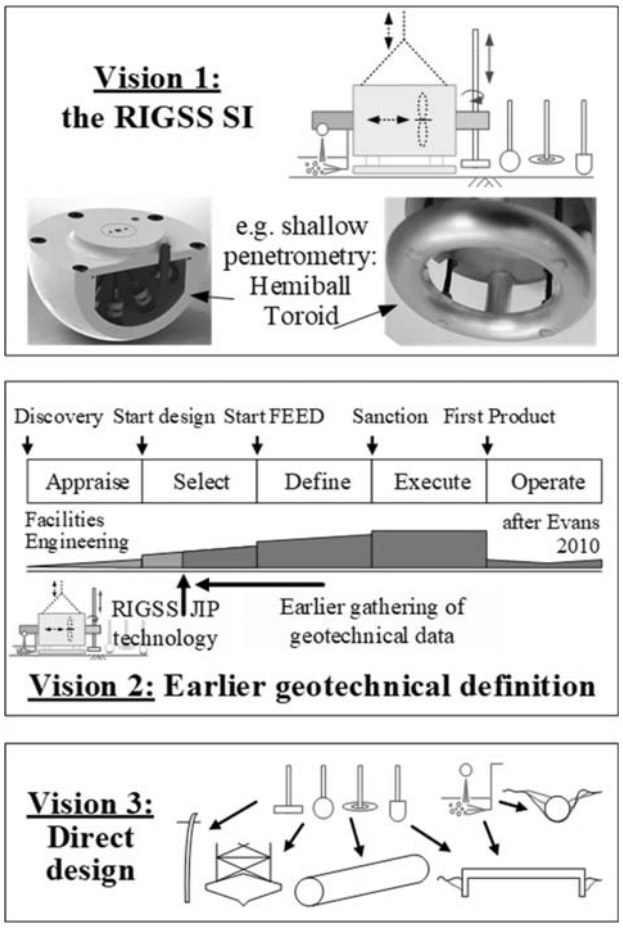

Figure 6. RIGSS JIP motivations (after White et al. 2017).

3.2 *Offshore box core testing*

Three types of 'shallow' penetrometers have been pursued within the RIGSS JIP. The toroidal and hemispherical ('hemiball') penetrometers were first described by Yan et al. (2011); more recently a ring-shaped variant on the toroid with a flat interface has been trialled. During a test, these devices are penetrated to a depth of less than a diameter (of toroidal bar, or hemiball) and are then subjected to one or more stages of rotation under maintained vertical load. Their shape and the interfacial sliding mode of failure resemble a pipeline, or other surface infrastructure such as mattresses or surface foundations.

Devices at box core scale have been developed and trialled in the UWA laboratory on reconstituted kaolin and carbonate silt samples. The system has also been taken offshore, for field trials on two surveys by the RIGSS JIP partners. The general design of the box core toroid penetrometer and the integrated data acquisition system are shown in Figure 7. The vertical force and torque on the penetrometer are monitored continuously, as are the pore pressures at multiple locations on the surface.

The soil-interface resistance is derived from the measurements, in terms of both total and effective

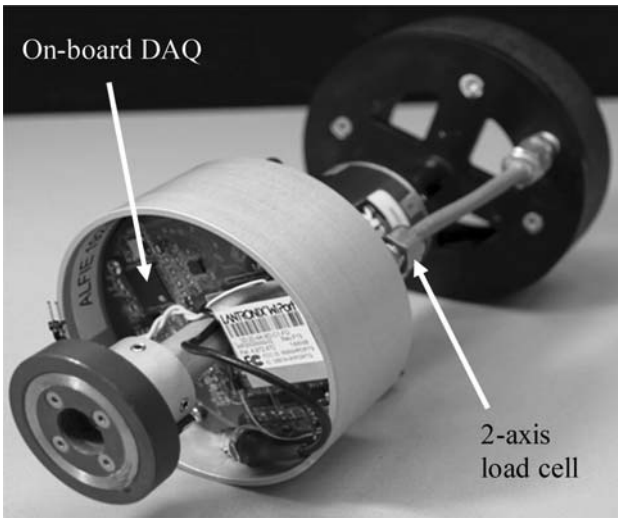

Figure 7. Toroid penetrometer with on-board DAQ and 2-axis load cell (vertical force and torque).

normal stresses. Dissipation stages allow the consolidation coefficient to be determined for fine-grained soils, while the timing of rotation stages may be varied to deduce both drained and undrained interface strengths.

Box-coring operations during one of the recent offshore trials are shown in Figure 8. By utilising multiple box core sleeves, sampling operations may be continued in parallel with shallow penetrometer testing within a previously recovered box core sample. Depending on the drainage properties of the samples, a full set of penetrometer tests in the box core might take 1–3 hours. If this aligns with the cycle time for the vessel transit between locations and box core recovery, then two sleeves can be alternated between sampling and testing.

The box core actuator system is shown during testing within a box core sleeve in Figure 9. Another approach is to take large diameter tube samples from the box cores, and perform tests off the sampling critical path using the arrangement shown in Figure 10.

The initial field trials provided valuable lessons to improve the procedures for deploying the tests and determining the best combination of tests to perform in a given soil type, to optimise the information gathered. The deck of a survey vessel is a challenging environment for performing precision testing, but vessel motions and changes in ambient temperature have had no detrimental effect on the

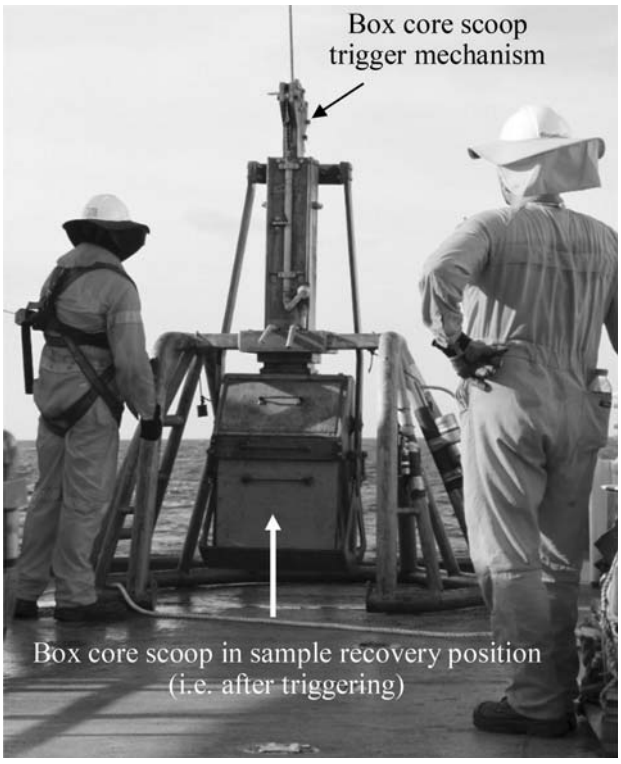

Figure 8. Typical box corer during sample recovery to deck.

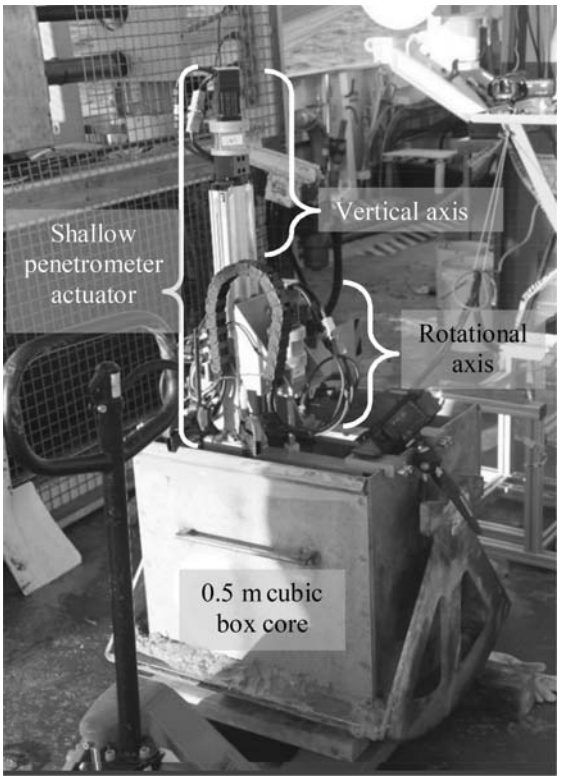

Figure 9. Shallow penetrometer system in 'box core' mode.

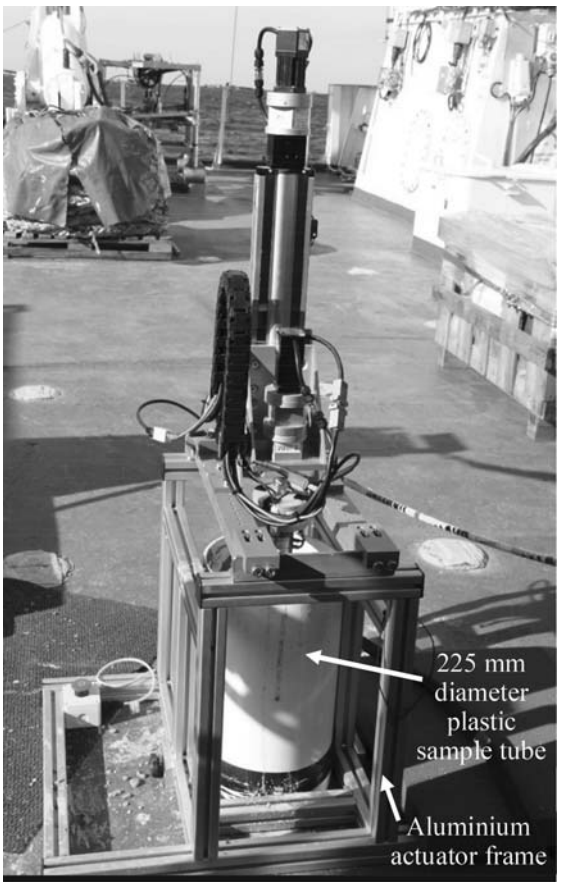

Figure 10. Shallow penetrometer system in 'tube sample' mode.

measurement quality emerging from the shallow penetrometer tests. To date, the testing equipment has required operation by a researcher familiar with the equipment and software controls. As the technology evolves, simpler systems will be created. We anticipate that shallow penetrometer testing could then be available on a basis similar to the existing Fugro DECKSCOUT and other box core penetrometer systems.

A typical set of results is used to illustrate the performance of the toroid penetrometer (Figure 7), operated in a box core sample of carbonate silt. The initial stage of a toroid test involves vertical penetration of the device to a depth of typically 20% of the diameter (Figure 11). The results are converted to a linear profile of undrained strength, s_u, using the bearing capacity model set out by Stanier & White (2015). In this approach, the bearing factor, N_c, is varied according to the depth and strength gradient, and a (small) adjustment is also made for soil buoyancy. An iterative process is required to reach s_u because N_c varies with s_u itself. The minimal noise in the measured data is equivalent to less than 0.1 kPa of strength (Figure 11).

After reaching the target depth, the vertical load on the penetrometer is maintained constant, while the excess pore pressure at the invert dissipates (Figure 12). The initial response—over the first five seconds of the dissipation—shows a rise in pore pressure, typical for dilatant soils. During the subsequent 10 minutes, the response follows closely the analytical model set out by Yan et al. (2017), based on numerical analysis. By matching the curves at the 50% dissipation point, a consolidation coefficient of 65 m^2/year is determined.

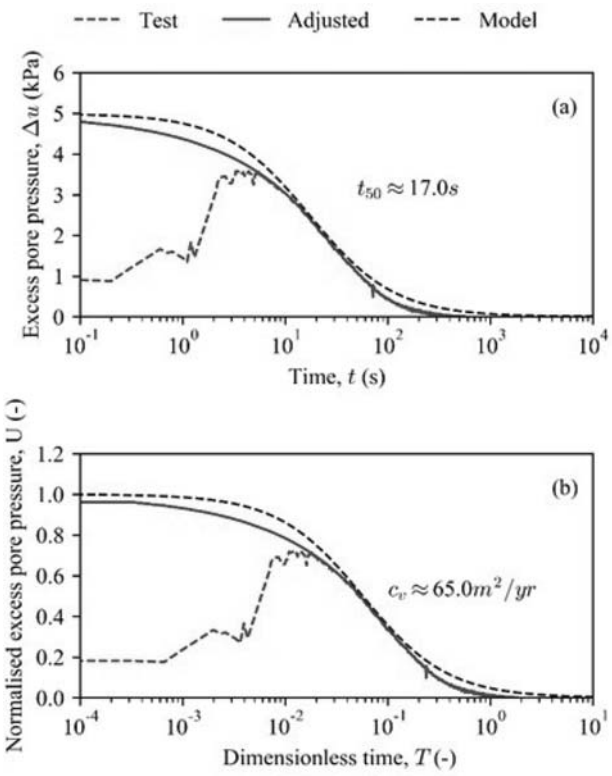

Figure 12. Toroid dissipation in carbonate silt: (a) measured response; and (b) interpreted coefficient of consolidation, c_v.

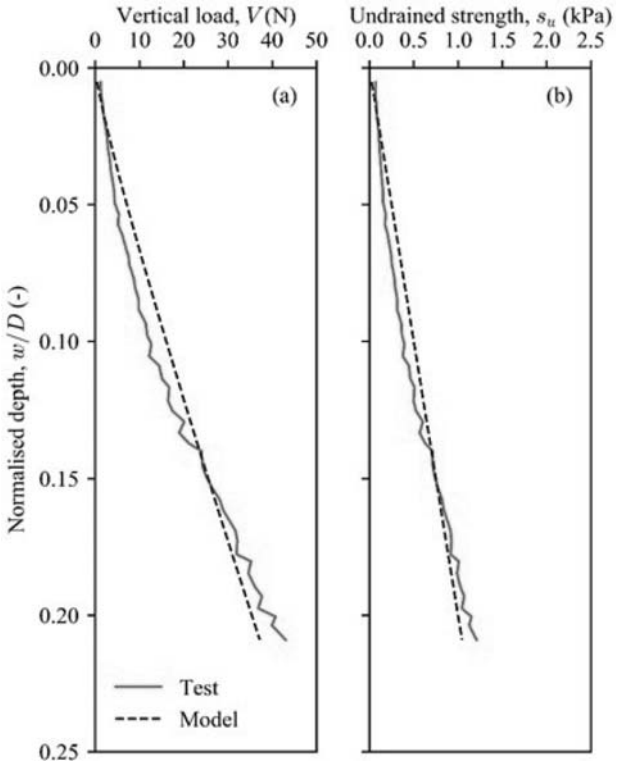

Figure 11. Fitting of measured toroid penetration response in carbonate silt with analytical model: (a) measured vertical load; and (b) interpreted profile of undrained shear strength, s_u.

The next stage of the test involves rotation of the toroid (Figure 13). Initially a high rotation rate is used to mobilise the undrained interface strength, including any initial peak but continuing towards the stable or residual value used in pipeline design. The rotation rate is then reduced by a factor of 10. Rotation continues as the resistance rises towards the drained limit, controlled by the interface friction angle.

The measured torque and vertical force are converted to interface friction ratio by dividing the torque by the effective radius (at which the resultant of the circumferential resistance acts) and multiplying the vertical force by a 'wedging factor' (White & Randolph 2007) to give the total normal force on the interface. The resulting interface friction ratio can be fitted by undrained and drained limits (Figure 13), which are key inputs to pipeline design. The rate of transition provides another indication of the consolidation coefficient, which may differ from the initial dissipation stage.

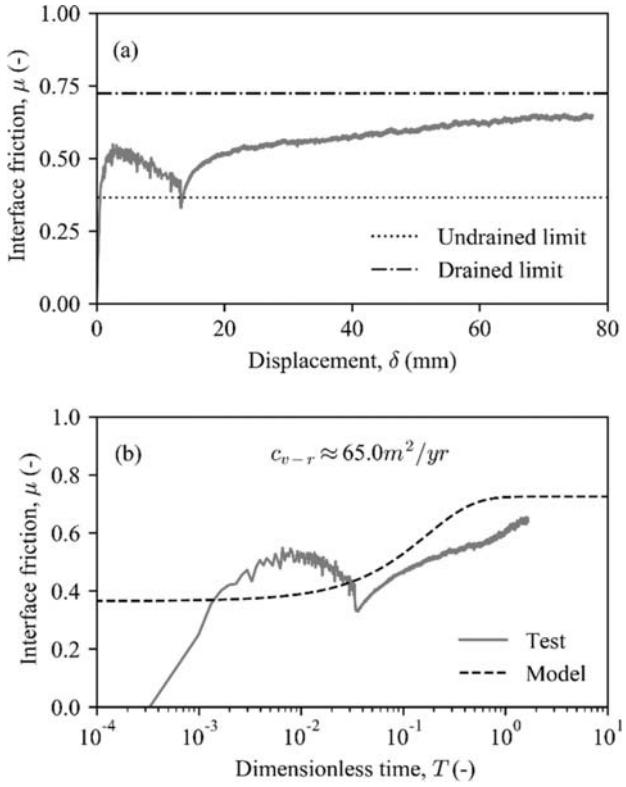

Figure 13. Toroid rotation in carbonate silt: evolution of interface friction, μ with (a) displacement; and (b) dimensionless time.

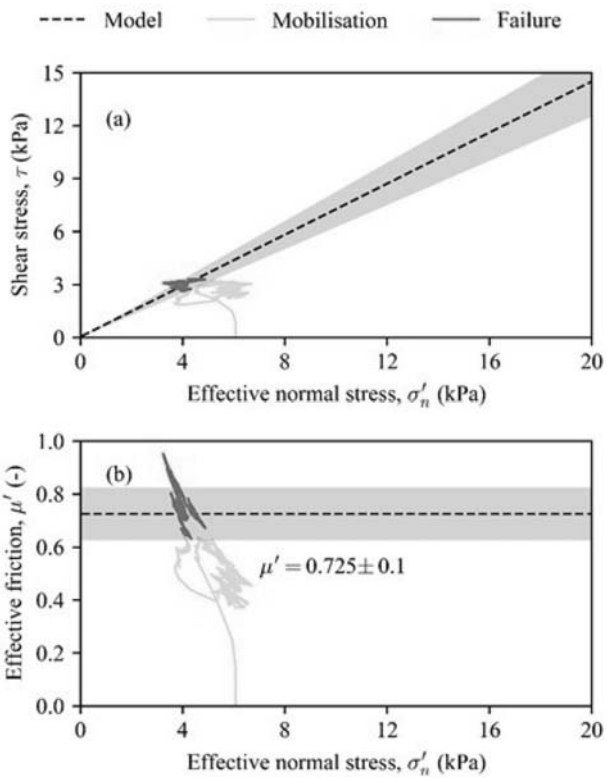

Figure 14. Toroid effective stress interpretation: (a) effective stress envelope; and (b) effective interface friction, μ'.

The undrained limit, if the soil has been normally consolidated under the penetrometer vertical load, is the 'c/p' or normally consolidated undrained strength ratio for the interface. The drained limit is $\tan(\delta_{res})$ where δ_{res} is the residual interface friction angle. This interpretation is aligned with conventions for pipeline design (White et al. 2017, DNVGL 2017).

The interface response can also be interpreted in effective stress terms using the pore pressure measurements (Figure 14). This provides useful confirmation of the drained friction, particularly if the tests are curtailed before pore pressure equilibrium is reached.

An additional type of test involves episodic rotations with intervening dissipations, which results in gradually increasing undrained resistance with each cycle (Yan et al. 2014, Boscardin & DeGroot 2015). The data may be interpreted within a consolidation framework, and used to support assessment of 'consolidation hardening' by which pipeline axial friction can rise through cycles of movement.

Overall, subject to a suitable box core sample being recoverable, a short series of shallow penetrometers tests (e.g. 2–3 tests performed over several hours), supplemented with conventional miniature T-bar (or ball) penetrometer tests, can provide all of the geotechnical strength and consolidation parameters required for pipeline design. We hope that these technologies will be taken forward by the RIGSS JIP partners over the coming years, allowing wider adoption in project practice.

4 FREE-FALL PENETROMETERS

4.1 *Introduction*

Free fall penetrometers (FFPs) may be divided into different classes, according to the sophistication of instrumentation (ranging from just accelerometers to fully instrumented with tip and shaft load cells and pore pressure sensors). Recent developments have included two-stage combined FFP systems where free-fall penetration is followed by static penetration. In addition, extended base FFPs have been explored for soft sediments, as discussed later. The discussion below describes different types of FFPs, and then summarises interpretation in fine-grained sediments.

4.2 *Probe geometry*

A variety off FFPs are shown in Figure 15. They vary in mass and geometry from the 52 mm diameter by 0.215 m long 0.7 kg expendable bottom penetrometer (XBP, Stoll & Akal 1999) to the

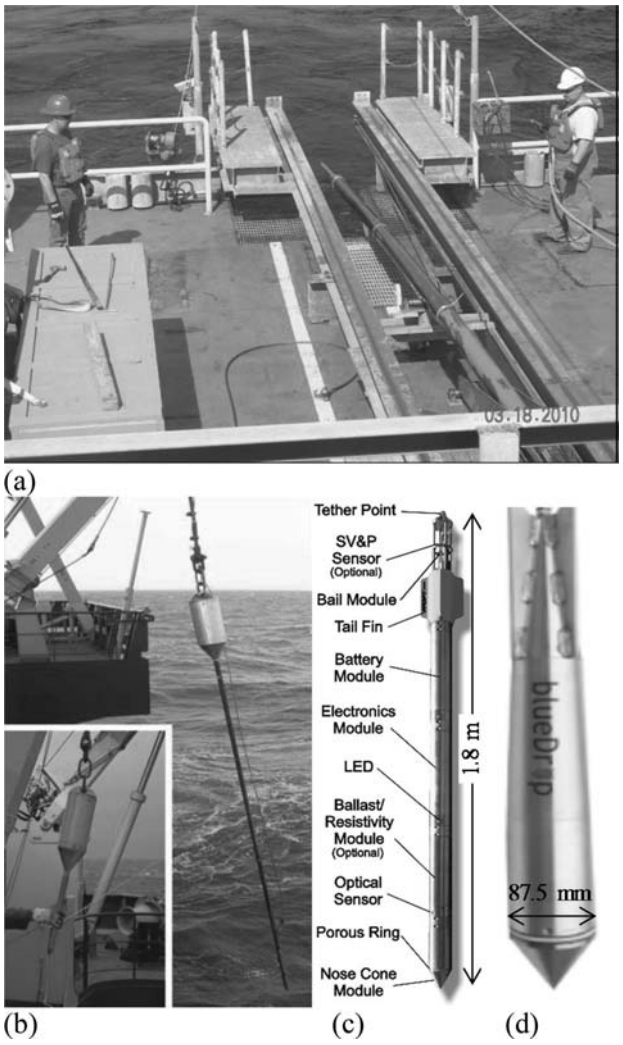

Figure 15. FFPs: (a) CPT Stinger (Young et al. 2011) (b) University of Bremen FFCPT shown in long and short (inset) modes (Stegman et al. 2006) (c) Brooke Ocean 'FFCPT-660' (Mosher et al. 2007) and (d) BlueDrop (Stark et al. 2014).

160 mm diameter (with a standard CPT tip) by 23 to 35 m long 3200 kg CPT-Stinger (Young et al. 2011). Penetration is generally proportional to mass (or momentum) per unit area (Peuchen et al. 2017), with the XBP generally penetrating less than 0.3 m, and the CPT-Stinger capable of reaching 20 m of dynamic penetration followed by another 15 m of static penetration.

A class of intermediate size probes capable of 4 to 6 m of penetration in soft clays, 1 to 2 m penetration in stiff clays and silts, and less than 0.5 m penetration in sands is seeing increased use for shallow investigations in soft materials. These penetrometers are relatively portable and can be used from survey size vessel with a high-speed winch for deployment and retrieval, with diameters of 100 to 200 mm, lengths of 1 to 6 m, and mass of 10 to 500 kg. They include:

- NAVFAC eXpendable Doppler Penetrometer (XDP) (Beard 1985, Orenberg et al. 1996, Thompson et al. 2002)
- Seabed Terminal Impact Naval Gauge (STING) (e.g. Mulhearn 2003)
- Brooke Ocean Free Fall CPT (FFCPT) (Furlong et al. 2006)
- Bremen Free Fall CPT (FFCPT) (Stegmann et al. 2006)
- NIMROD (Stark et al. 2009)
- LIRmeter (Stephan et al. 2011)
- BlueDrop (Stark et al. 2014)
- Graviprobe (Geirnaert et al. 2013)
- Instrumented Free-Fall Sphere (IFFS) (Morton et al. 2016a)
- SEADART1 (Peuchen et al. 2017)

4.3 *Sensors*

Historically FFPs were only equipped for acceleration or velocity measurements. With the need for higher quality measurements of the location of the seabed, soil strength, as well as inferences of soil type, additional sensors such as optical sensors, tip stress, sleeve friction, penetration pore pressure, and resistivity have been added to probes.

The most efficient means of FFP operation is whereby the instrumentation package has sufficient power and storage for a series of tests. In a continuous test mode, where the penetrometer is repeatedly deployed and retrieved, the instrumentation package should have storage and battery capabilities for about 12 hours of testing. After this the package can be removed from the penetrometer for battery recharging and data download, or alternatively the package could be replaced with a spare system, allowing testing to continue without delay.

Modern data acquisition systems allow for this mode of operation. For example, the UWA instrumentation package shown in Figure 16 is sufficiently compact to fit within the smallest FFPs, but allows for sampling rates of up to 500 kHz and at a practical sampling rate of 1.5 kHz for FFP tests, up to 225 hours of data storage and 20 hours of continued use before the batteries require recharging.

All FFPs measure acceleration along an axis aligned with the body of the FFP (although often sensors with different measurement ranges are included to optimise resolution). The UWA instrumentation package shown in Figure 16 is an inertial measurement unit (IMU), which measures acceleration along each axis of a Cartesian coordinate system and provides independent measurements of the rotations about each axis of the same coordinate system. Transforming the measurements from the body reference frame of the FFP (which will be changing during an FFP test if the

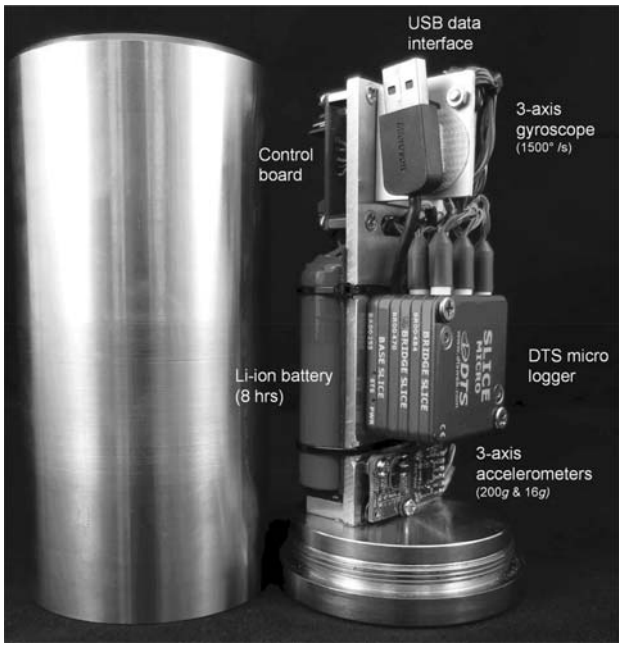

Figure 16. UWA inertial measurement unit (IMU).

FFP tilts by varying amounts) to a fixed reference frame avoids the difficulty in identifying the component of the acceleration signal that is due to FFP rotation from that due to changing acceleration (Blake et al. 2016).

O'Loughlin et al. (2014) showed that the corrections using this approach become appreciable at tilts in excess of 10°. Conical shaped penetrometers appear to tilt less than this threshold (Kopf et al. 2007), but for other penetrometers, particularly the free-fall sphere penetrometer (described later), the tilts are likely to be much higher, such that an IMU approach is required.

4.4 *Interpretation using acceleration data*

The ultimate objective of a FFP test in fine-grained material is to assess the undrained shear strength s_u. This may be derived from the tip resistance in the conventional way as for a static CPT, but with appropriate allowance for the high strain rates resulting from the high velocity penetration. Ideally, the FFP should measure the tip resistance directly. However, for FFPs that do not include a tip load cell, estimation of the tip resistance involves a number of steps and uncertainties.

The tip resistance may be derived from the penetrometer mass, m, times the measured acceleration, a = v(dv/dz) according to

$$q_{t,FFP} = \frac{W_b - mv(dv/dz) - Q_s - F_D - F_b}{A_{tip}} \quad (1)$$

where v is the FFP velocity, z the penetration, W_b the submerged weight of the FFP in water, Q_s the frictional resistance along the shaft, F_D the drag resistance (due to soil inertia), F_b the buoyancy force equal to the effective weight of the displaced soil and A_{tip} the cross-sectional area of the tip (True 1976, Rocker 1985, O'Loughlin et al. 2004, Chow et al. 2017).

The challenge with this approach is in correctly identifying and quantifying the magnitude of the various terms in Equation (1). A further complication is that, since the undrained shear strength (derived from the tip pressure $q_{t,FFP}$) contributes towards the shaft resistance, an iterative approach is needed in solving for the tip resistance. This may be avoided for extended base FFPs such as the free-fall sphere and STING, since the shaft resistance may be excluded from Equation (1). However, it may then be necessary to consider the additional soil mass that moves with the base (Morton et al. 2016b).

4.4.1 *Hydrodynamic and soil drag*

Soil drag resistance can dominate interpretation of strength in weak seabeds at shallow embedment, and accounting for this parameter is necessary for accurate strength assessments as well as in probe design. Soil drag is calculated in the same manner as for hydrodynamic drag, as

$$F_D = 0.5 C_d \rho_s A_{tip} v^2 \quad (2)$$

where ρ_s is the saturated density of the soil and C_D is the drag coefficient, the value of which depends on the penetrometer geometry. The density must be estimated (since samples are not taken) and there is uncertainty in the drag coefficient.

Consideration of the acceleration trace during the free-fall in water phase allows the fluid drag characteristics, and its variation with Reynolds number for a particular geometry, to be established (Morton et al. 2016a, O'Beirne et al. 2017). It is common to estimate the soil drag coefficient as the same as the fluid drag coefficient, which tends to vary from about 0.15 (increasing with L/D) for cylindrical penetrometers with hemispherical tips, to about 0.26 for spheres.

If the fluid and soil drag coefficient are assumed equal, the influence of the tether on drag characteristics should be considered. Depending on probe mass, geometry, fall height through water, and tether characteristics, tethered terminal velocities may be half or less than untethered velocities, as indicated by offshore data in Figure 17. Upon seabed impact the tether may tend to go slack, changing the drag resistance implied by the probe impact velocity.

4.4.2 *Shaft frictional resistance*

For probes that only measure acceleration or velocity, the friction along the side of the probe must be subtracted from the total resistance to

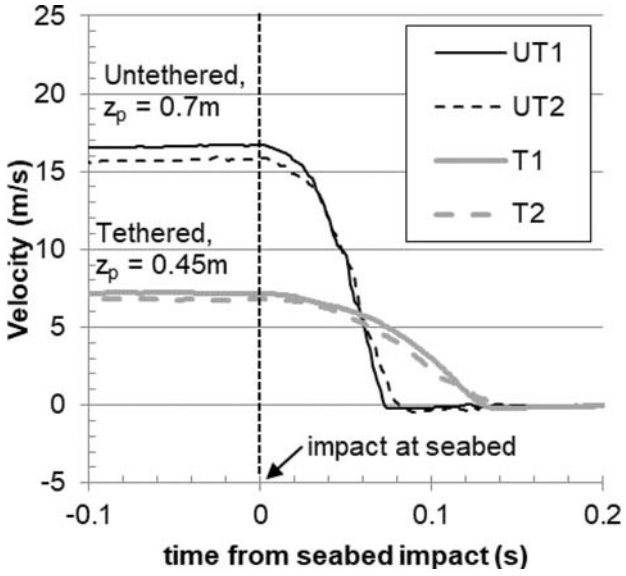

Figure 17. Influence of tethering on penetration of NAVFAC XDP drop through 30 m of water into a low plasticity clay with s_u of 10 to 20 kPa in the upper 0.75 m.

assess tip resistance. Shaft friction on the side can be estimated based on the undrained strength through an adhesion factor, α, which is commonly assumed to be the inverse of the soil sensitivity. The total shaft friction at any given penetration is:

$$Q_s = \sum \Delta A_{shaft} R_{f,shaft} \alpha s_u \tag{3}$$

The significant uncertainty in soil sensitivity (or α), and how that varies with depth, will propagate through to the accuracy of the estimated tip resistance. The shaft friction is also found to exhibit much higher rate effects than the tip resistance (as discussed later) and hence a higher rate parameter $R_{f,shaft}$ (Steiner et al. 2014, Chow et al. 2017). The uncertainty in both the soil sensitivity and $R_{f,shaft}$ is the most significant factor for accurate estimation of soil strength using the accelerometer measurement.

4.5 *Cone tip resistance and derivation of s_u*

Improved estimation of soil strength can be obtained by measuring the FFP tip resistance directly with a load cell. Interpretation is similar to that for a static CPT, with the additional need to deduct drag resistance and to discount the soil strength for strain rate effects, according to:

$$s_u = \frac{q_{c,FFP} - q_D + u_2(1-\alpha_{cone}) - \sigma_{v0}}{R_{f,tip} N_{kt}} = \frac{q_{net,d}}{R_{f,tip} N_{kt}} \sim \frac{q_{net,s}}{N_{kt}} \tag{4}$$

where $q_{c,FFP}$ is the measured tip resistance, u_2 the pore pressure measured or estimated at the cone shoulder, α_{cone} the unequal area ratio, σ_{vo} the overburden stress, q_D the drag resistance (equivalent to F_D/A_{tip} from Equation (1)), $R_{f,tip}$ the strain rate factor for tip resistance, N_{kt} the cone factor, $q_{net,d}$ the resulting dynamic net cone resistance and $q_{net,s}$ the static net cone resistance from a conventional CPT.

4.6 *Viscous rate effects*

The extremely high penetration velocity of an FFP (especially at shallow depth) leads to very high strain rates in the soil that will enhance the soil strength beyond nominally undrained values. The effect of strain rate may be modelled using either a semi-logarithmic (or inverse hyperbolic sine function) or power law (including the Herschel-Bulkley formulation). The simple power law of

$$R_{f,tip} = \left(\frac{\dot{\gamma}}{\dot{\gamma}_{ref}}\right)^{\beta} = \left(\frac{v/D}{(v/D)_{ref}}\right)^{\beta} \geq 1 \tag{5}$$

has generally been adopted as it is found to capture rate effects better than logarithmic functions over large ranges of strain rate (Biscontin & Pestana 2001). Here $\dot{\gamma}$ is the strain rate, $\dot{\gamma}_{ref}$ the reference strain rate associated with the reference value of undrained shear strength and β a strain rate parameter. The average strain rate may be linked directly to the normalised velocity, v/D. Due to the different rate effects observed for the tip and shaft resistance (see later, Figure 19) different strain rate parameters, β_{tip} and β_{shaft} are recommended for estimating $R_{f,shaft}$ and $R_{f,tip}$ in Equations (3) and (4) respectively.

The reference strain rate, and hence selection of v_{ref} and D_{ref}, should correspond to nominally undrained conditions, similar to those that would develop in a static cone penetrometer test. For instance selection of v_{ref} = 20 mm/s and D_{ref} = 35.7 mm would result in a strength that would be comparable to that measured by a 10 cm^2 cone penetrated at the usual 20 mm/s. For an FFP with diameter of 100 mm, travelling at velocity, v = 10 m/s, v/D = 100 s^{-1}, two orders of magnitude higher than in the static 10 cm^2 cone test. For this magnitude variation in strain rate, the strain rate parameter β_{tip} is typically in the range 0.03 to 0.09 for tip resistance (Lehane et al. 2009, O'Loughlin et al. 2013, 2016, Chow et al. 2017).

4.7 *Example interpretation from test data*

An example interpretation from centrifuge experiments in kaolin clay (Chow et al. 2017) is provided in Figure 18 to Figure 20. The interpretation based solely on acceleration measurements (but with

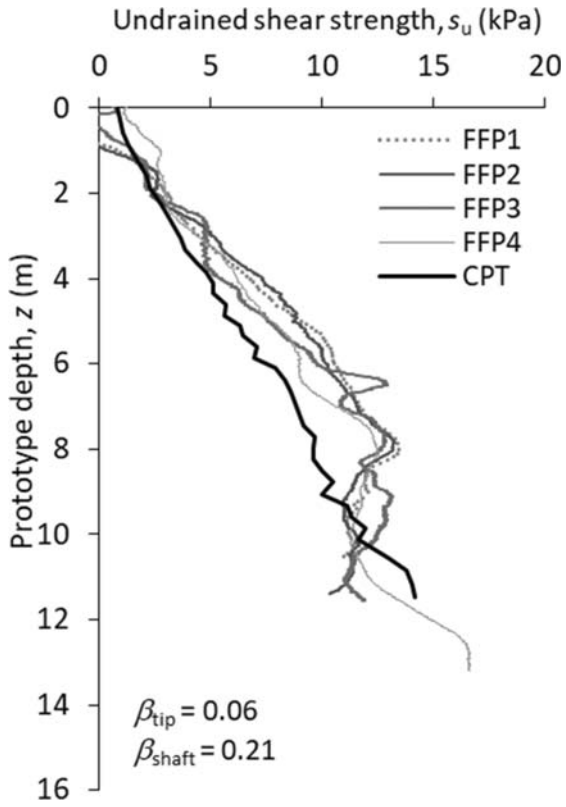

Figure 18. Estimated s_u profiles using the accelerometer method (after Chow et al. 2017).

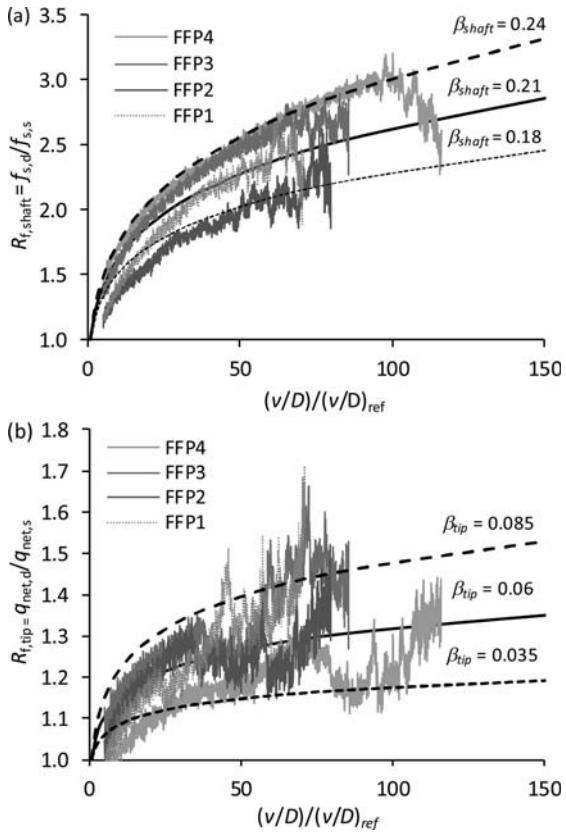

Figure 19. Back-fitted rate parameters for (a) shaft resistance and (b) net tip resistance (after Chow et al. 2017).

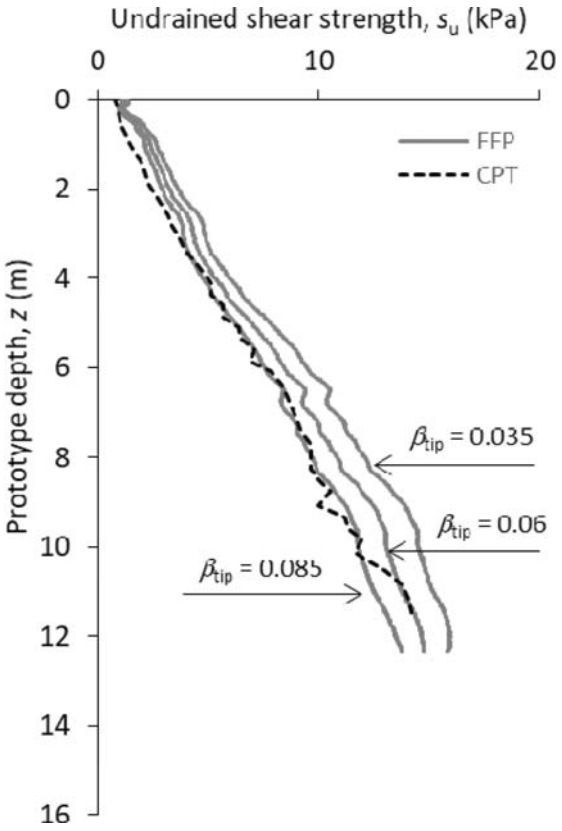

Figure 20. Deduceds_u profiles using tip load cell (after Chow et al. 2017).

no account taken of any 'tethering' effects since these are negligible for the centrifuge model test) underestimates the strength deduced from static CPTs by approximately 50%, even when separate strain rate parameters (β_{tip} and β_{shaft}) are applied, as established in direct measurements from the tip and shaft load cells of the FFP (see Figure 19). This large discrepancy is caused by the uncertainty in estimating the dynamic shaft resistance reliably (Chow et al. 2017).

Figure 20 shows (for the same Chow et al. 2017 centrifuge tests) that when the interpretation is based on the tip load cell and u_2 pore pressure measurements, s_u values determined from static CPTs and FFP tests are essentially indistinguishable. The interpretation on Figure 20 uses a median $\beta_{tip} = 0.06$, with variations in β_{tip} (reducing to $\beta_{tip} = 0.035$ and increasing to $\beta_{tip} = 0.085$) leading to changes in the FFP s_u interpretation that vary by less than ±10%. Interestingly, the u_2 excess pore pressure response was mainly negative in the FFP tests and positive in the static CPTs, although the measured (negative) u_2 without adjustment was needed in Equation (4) for correcting the unequal area effect in order to provide the agreement in Figure 20.

The negative u_2 measured during the dynamic penetration has been attributed to local effects due

to the cone geometry and position of the u_2 sensor (Chow et al. 2014). The phenomenon may be considered a result of Bernoulli effects, as illustrated by computational fluid dynamics analyses for free fall in water (Lucking et al. 2017, Mumtaz et al. 2018). Negative u_2 values following embedment were also found in large deformation finite element analyses for soils that show strain rate dependency of strength (Sabetamal et al. 2016). This requires further experimental validation, and is particularly important if FFPs are to be interpreted to provide Robertson-style soil behaviour types.

4.8 *Penetrometer shape*

Where accurate determination of s_u at shallow depths (e.g. < 1 m) is required, there may be benefits in employing 'extended base' FFPs. Examples include the plate-tipped STING (Mulhearn 2003, Fawaz et al. 2016; Chow & Airey 2014; see Figure 21a) and the free-fall sphere (Morton et al. 2016a, b; see Figure 21b). Due to the relatively large tip area of these FFPs, drag resistance becomes a significant and often dominating component of the soil resistance.

In addition to the better resolution in s_u permitted by the larger tip area, there is essentially no shaft resistance on an extended base FFP, so that the complex calculation of dynamic shaft resistance is avoided. This allows s_u to be determined indirectly from the acceleration measurements, meaning that this class of FFP does not require load cell measurements.

Example interpreted s_u profiles for the free-fall sphere are provided in Figure 22 for a lake-bed clay in Northern Ireland and a nearshore clay in the Firth of Clyde, off the West coast of Scotland. Significant penetrations were achieved, particularly in the very soft lake-bed clay, using impact velocities typically in the range 4 to 8 m/s.

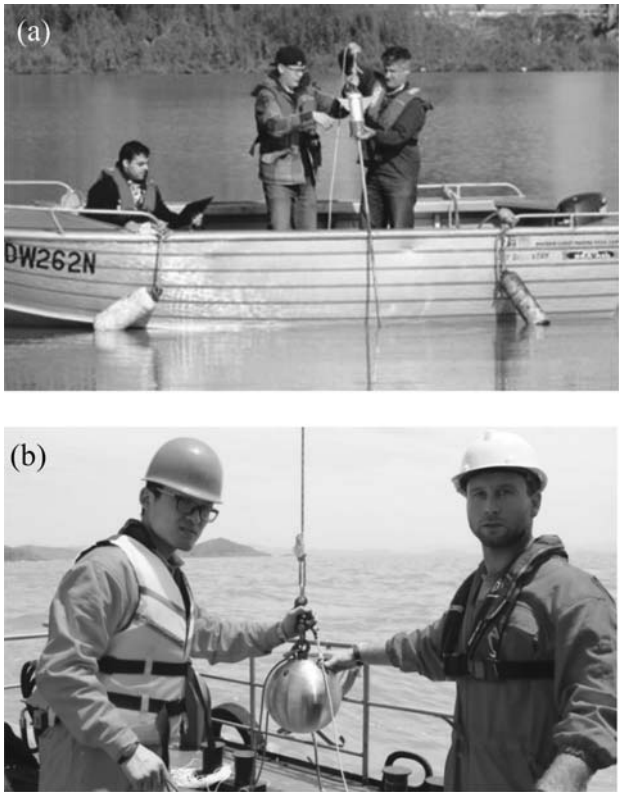

Figure 21. Extended base FFPs: (a) STING (Fawaz et al. 2016), (b) free-fall sphere.

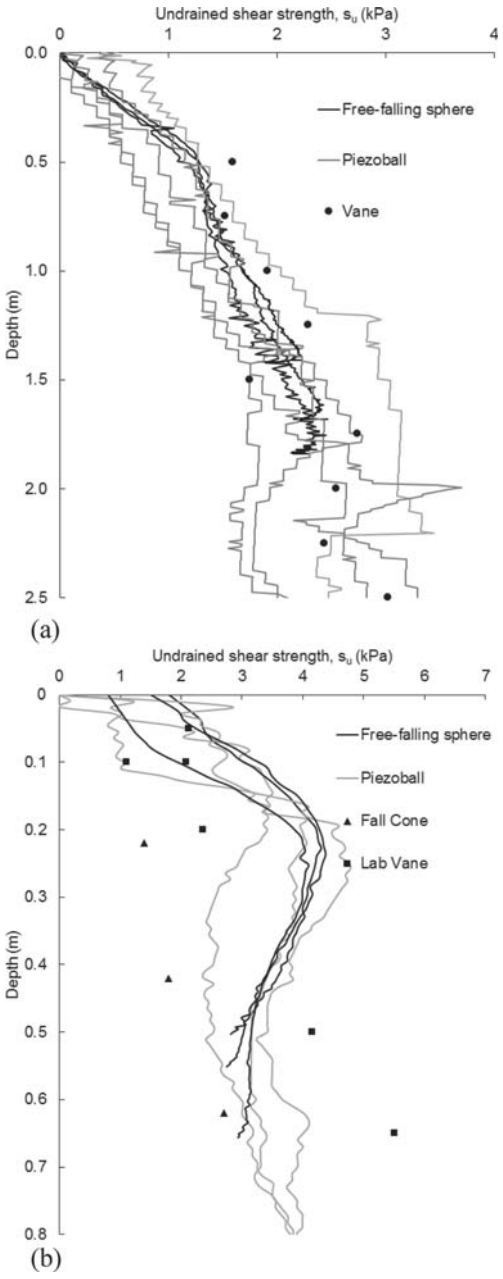

Figure 22. Comparison of undrained shear strength profiles derived from free-fall sphere acceleration data and push-in piezoball penetration resistance: (a) a lake site (Lough Erne, Northern Ireland) and (b) a nearshore site (Firth of Clyde, Scotland) (Morton et al. 2016a).

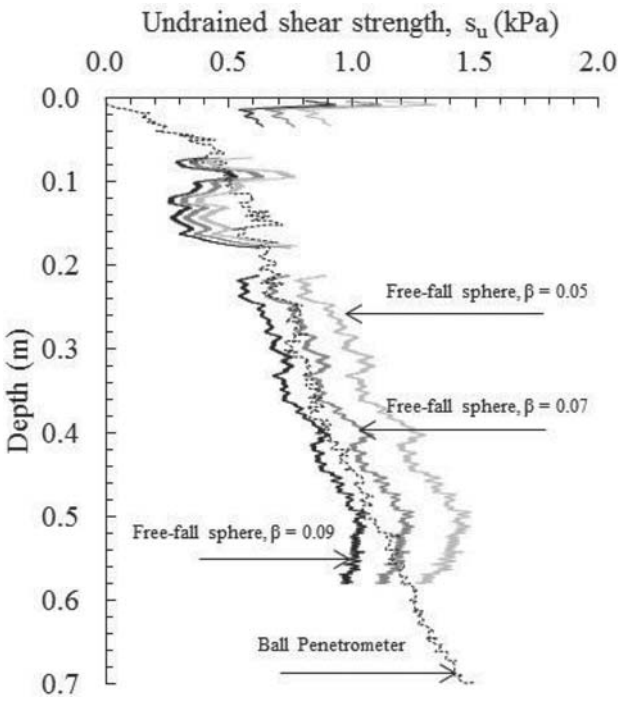

Figure 23. Sensitivity of interpreted s_u profiles to changes in the strain rate parameter (Morton et al. 2016b).

The free-fall sphere s_u profiles are seen to agree well with static piezoball tests on Figure 22, where the same piezoball factor was used (at each site) to calculate s_u from the static and FFP net resistance, and the same strain rate parameter, $\beta = 0.07$ and drag coefficient, $C_d = 0.26$ were used for both sites. Interpretation of the Clyde tests—static and free-fall—required adjustment of the bearing capacity factor at shallow depths, as discussed in the following section.

The sensitivity to uncertainty in β is demonstrated by Figure 23, which compares centrifuge s_u profiles from free-fall sphere tests with equivalent static profiles for a reconstituted carbonate clay from Laminaria (Timor Sea); β is varied by ± 0.02 from the base case $\beta = 0.07$ (used for both the centrifuge and field tests). The lower bound $\beta = 0.05$ corresponds with the largest departure from the base case profile established using $\beta = 0.07$, although by less than 20%. This uncertainty is comparable to the differences that are commonly linked to uncertainty between different laboratory strength tests (Bienen et al. 2010).

4.8.1 *Shallow embedment correction factors*

For large diameter penetrometers, it is necessary to modify the bearing capacity factor, N_{FFP}, for shallow embedment (e.g. Rocker 1985, Aubeny & Shi 2006, White et al. 2010, Morton et al. 2016a). The bearing capacity factor tends to increase from the shallow foundation factor at the seabed interface to the deep factor at depth. In soils with a constant strength, the deep factor is typically reached within approximately four diameters (depending on the normalised strength ratio $s_u/\gamma'D$). The shape of the transition to 'deep' conditions will be influenced by the strength gradient and unit weight of the soil (e.g. Stanier & White 2015).

4.9 *Summary comments on FFPs*

In spite of the cost-effectiveness of free-fall penetrometers (FFPs), compared with mobilising a seabed frame to conduct static penetrometer tests, the quality and usefulness of the data acquired need to be considered carefully within the context of the site investigation objectives. In the early stages of characterising the seabed, and particularly for spatially extensive surveys for pipeline routing, it may be sufficient to acquire data that merely distinguishes rock (or cemented) outcrops, from sandy deposits all the way down to fine-grained sediments of different strengths. Where soft sediments can be anticipated, quantitative strength data in the upper metre or so would be useful even at a preliminary SI stage.

Lightly instrumented FFPs are sufficient for primary categorisation of the seabed material. Penetration of the seabed will be minimal for cemented crusts, and unlikely to exceed a fraction of a metre in most types of coarse-grained (silty sands and coarser) material, regardless of the mineralogy or relative density (Stark et al. 2012). This may be sufficient during concept selection and pipeline routing studies. However, where anchors are anticipated, it may be difficult to distinguish between sandy sediments sufficiently thick for good drag anchor performance, and superficial sand layers overlying rock, resulting in much less certain anchor holding capacity.

As in other methods of site investigation, the guiding principle must be to ensure free-fall penetration (and ideally deduction of the tip resistance profile) to depths compatible with the design target. In fine-grained sediments, where quantitative assessment of the shear strength profile is important, the required accuracy needs to be considered in choosing the type of FFP.

The new generation of combined dynamic and static penetrometers, where calibration of dynamic effects can be achieved through overlapping zones of dynamic and static data (Young et al. 2011, Randolph 2016), are an excellent cost-effective approach for moderate-sized foundation or anchoring solutions. However, the deployment of such systems requires prior knowledge that the sediments are fine-grained and relatively low strength, excluding any sandy layers or other obstructions. Additionally, since calibration with

respect to rate factors etc. is sensitive to the soil type, the correction may not be valid over the full depth of dynamic penetration.

For assessing the shear strength of the upper 1 m or so of the seabed, smaller FFPs, either free-falling piezocones or extended base devices, are more cost effective than larger FFPs. Ideally one or two independent static CPTs should be included for calibration, balancing the operational efficiency of FFP testing with the improved confidence and accuracy from calibration against data from static penetrometer tests (Steiner et al. 2012). Overall, though, for free-falling cone penetrometers, direct measurement of tip resistance, albeit under dynamic conditions, is essential, given the uncertainties associated with drag resistance at shallow depths and estimating the rate-enhanced shaft resistance.

5 APPLICATION OF PENETROMETER DATA IN DESIGN

5.1 *Trends of indirect and direct penetrometer correlations*

Along with the development in geotechnical site investigation, which routinely includes in situ penetrometer testing, methods to use the acquired data more directly for foundation design have become widespread. The boundary between 'indirect' and 'direct' is not clear cut, but here the former is restricted to deriving simplified profiles of fundamental soil properties such as shear strength or the equivalent (friction angle or relative density) for free-draining sediments. By contrast, direct design approaches derive foundation design parameters from the CPT data, such as modern approaches for axial pile capacity in sand as detailed in Recommended Practice 2Geo of the American Petroleum Institute (API 2011).

For shallow foundations there are a range of approaches, from directly correlating the penetrometer resistance with the foundation capacity (e.g. Lee and Randolph 2011, Pucker et al. 2013, Bienen et al. 2015), using the cone tip resistance as input in numerical analysis (e.g. Schneider et al. 2018), to inferring the soil type from the penetrometer data and using the deduced strength in traditional bearing capacity predictions (e.g. Safinus 2015). The last approach might really be considered as 'indirect' except that the method to extract the layering and strength properties is fully automated.

As with any other engineering application, though, the prediction method cannot increase the quality or relevance of the input data. Hence, in order to obtain accurate predictions, sufficient high quality penetrometer data are required at the target location in combination with a sound correlation method. Furthermore, while computational power is ever increasing, the target application may still limit what is practicable for routine design (e.g. direct input of a CPT profile into large deformation numerical analysis to obtain a jack-up spudcan load-penetration curve).

Jack-up spudcans have been the focus of a number of proposed correlation methods recently, as a result of often sparse site investigation data available for a priori predictions and relatively high proportion of incidents and accidents (Osborne et al. 2006, Hunt 2008, Jack et al. 2013). The proposed approaches to using penetrometer data in design differ in the detailed treatment of soil behaviour, but also in the computational effort required.

Assigning soil layers in the geotechnical design process retains an element of subjectivity that is difficult to remove. Automatic identification of primary geotechnical layers from in situ penetrometer data, for example following Robertson's approach of categorising the soil behaviour type index ($I_{c,RW}$ – Robertson & Wride 1998, I_B – Robertson 2016) to assign strength values, feeds into a top-down calculation to arrive at the predicted spudcan penetration resistance profile (Safinus 2015). The method offers the advantage of capturing the evolution of the soil profile (and plug) with spudcan penetration, with an example provided in Figure 24. Limitations of the approach include the reliance on correlations of questionable accuracy to infer soil unit weight and strength parameters for carbonate sediments, in particular sands.

The cone tip resistance profile can also be used directly to obtain the spudcan load-penetration curve via a correlation factor. With the bearing capacity factor N_c of a deeply penetrated foundation of approximately 9.0 and recommended average value of N_{kt} of approximately 13.5, a correlation factor of 0.67 is arrived at for clay (Osborne et al. 2011). Similar direct correlation factors for spudcans penetrating into siliceous and uncemented carbonate sand are provided in Pucker et al. (2013) and Bienen et al. (2012), respectively. This direct correlation method has been benchmarked against field data from offshore wind installations on sand sites in the North Sea (Edwards et al. 2013), with similar performance to predictions based on ISO (2012, previously SNAME) – see Figure 25.

Layered soil profiles introduce the issue of scaling, as a large size object such as a spudcan will have an averaging effect, while a penetrometer will resolve finer detail of strength variation. In the guidelines originating from the InSafe JIP (Osborne et al. 2011) a strength averaging approach is adopted to account for the apparent size effect.

Two other aspects of scale are important. The first involves differences in drainage regime for the

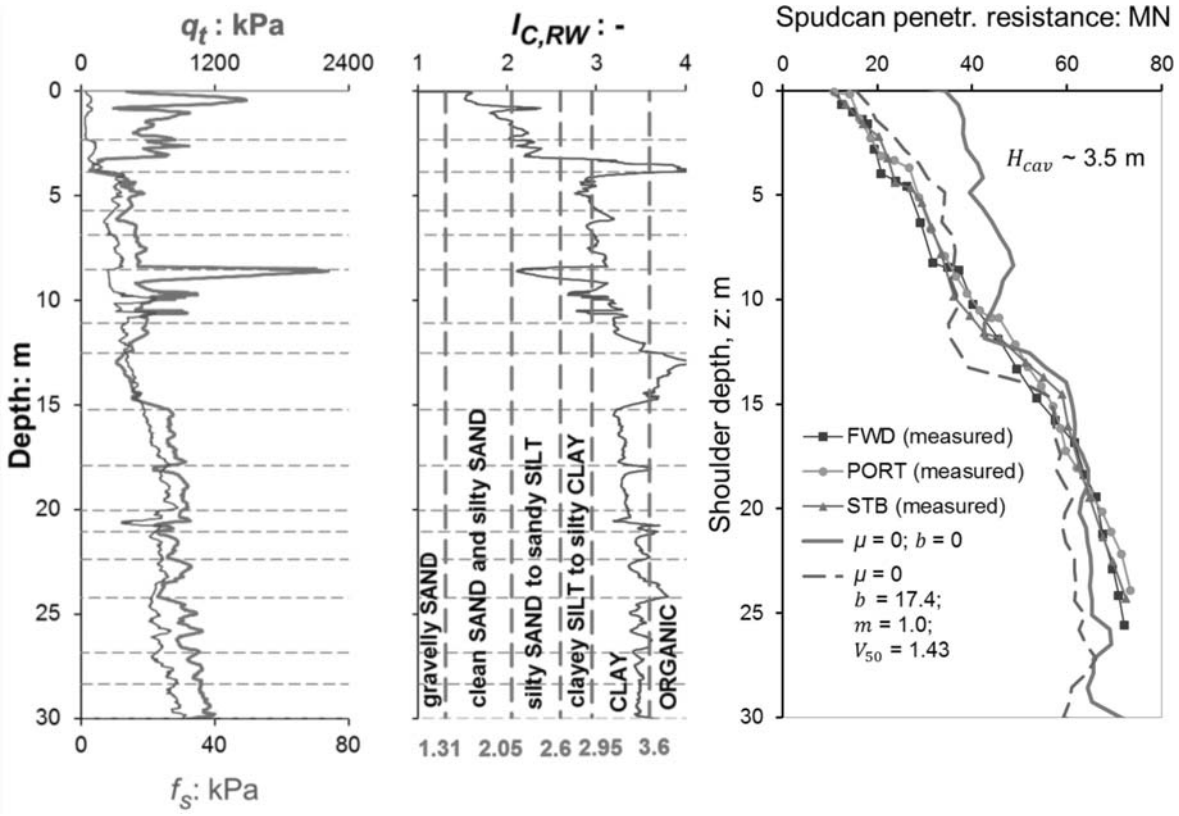

Figure 24. Spudcan load-penetration curve prediction (after Safinus 2015).

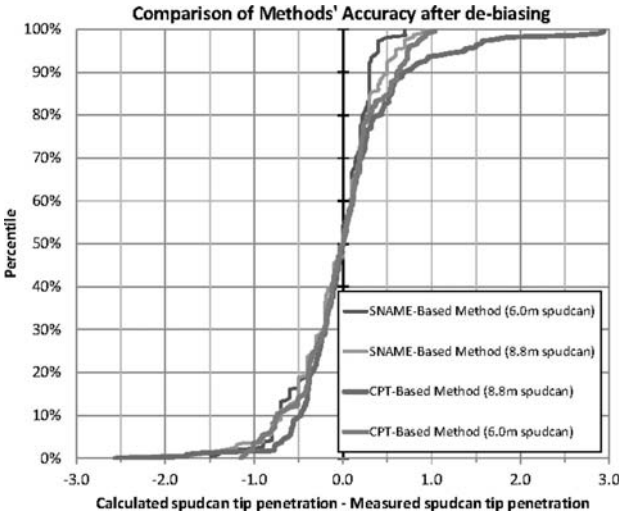

Figure 25. Comparison of the performance of direct CPT correlation and predictions based on ISO (2012).

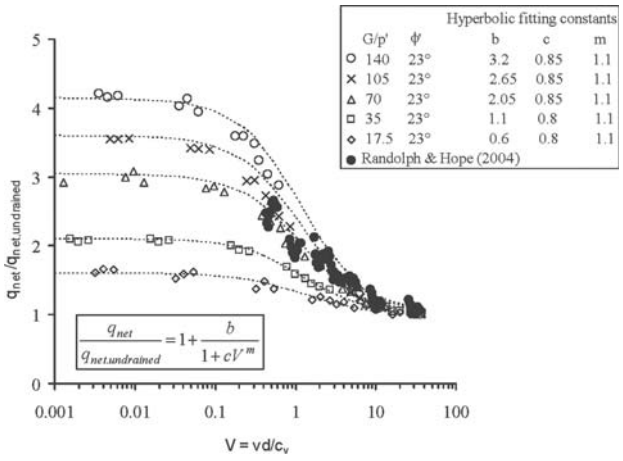

Figure 26. Normalised enhancement of penetration resistance with non-dimensional velocity.

penetrating object compared with a penetrometer. The second concerns the different modes of failure arising in strongly stratified profiles, i.e. with sand layers interleaved with layers of fine grained sediments.

The drainage regime may be close to fully undrained for a large diameter foundation such as a penetrating spudcan, even in sediments that are essentially free-draining during a penetrometer test. These differences in drainage characteristics lead to variations in the mobilised resistance, as illustrated in Figure 4 and Figure 5. The guidelines resulting from the InSafe JIP (Osborne et al. 2011) recommend modifying the factor of N_c/N_{kt} by the ratio between spudcan and penetrometer 'q_{net}' values arising from partial drainage, as illustrated in Figure 26. Values of q_{net} are estimated from the consolidation curves for normalised velocities

$V = vD/c_v$ using the spudcan and penetrometer diameters.

Erbrich (2005), Amodio et al. (2015) and Erbrich et al. (2015) provide detailed discussion of the effect of drainage on spudcan response, including additional consideration of cyclic degradation of the carbonate soils prevalent in areas of oil and gas developments offshore Australia (North West Shelf, Bass Strait).

With respect to the different penetration mechanisms that occur in stratified profiles, some methods (e.g. Safinus 2015) take specific account of effects such as squeezing of soft material overlying stronger material, punch-through for 'sand over clay' profiles, and allowance for a plug of stronger soil being trapped ahead of the penetrating spudcan. Simpler approaches are based on direct correlation to obtain an estimate of the spudcan load-penetration curve from the cone tip resistance, including consideration of the averaging distance. A method of this type is described by Bienen et al. (2015) for stratified 'sand over clay' profiles that may bear the risk of punch-through failure.

Jack-up spudcans are only one application example, of course, with other relevant applications affected by soil stratification including laterally loaded piles and anchor response. The example provided in Schneider et al. (2018) illustrates the merit of using in situ penetrometer data as input into numerical analysis to obtain foundation capacity in soil with layering. Another example, but for suction caisson capacity, is given below.

This section has illustrated a range of approaches to utilise penetrometer data in design. Penetrometer based methods need to be evaluated alongside more traditional design approaches, using data from actual foundation performance, in order to improve confidence in the methods and encourage further evolution. This also offers the opportunity of evidence-based selection of the most economical prediction method, balancing an appropriate level of sophistication relative to the available input data.

5.2 *Direct and indirect application of penetrometer data in numerical analysis*

Most foundation and anchor design is based on 'interpreted' penetrometer data, where simplified piecewise linear variations of shear strength are fitted to profiles of net penetrometer tip resistance using appropriate bearing (i.e. cone, T-bar, ball, etc.) factors. Schneider et al. (2018) discuss the potential errors that may arise from this approach, comparing results obtained using either an idealised strength profile, or the actual variation of (factored) net cone resistance.

Figure 27 shows the strength profile deduced from CPT data using a cone factor of $N_{kt} = 13.5$, from the second example (C6) considered in Schneider et al. (2018). The CPT profile is compared with the corresponding idealised s_u profile of $s_u = \max(1.9, 1.43z)$ kPa, where z is the depth in m. Corresponding ratios of the idealised and 'direct' (i.e. from the CPT profile) shear strengths are shown in Figure 28.

The idealised strength profile shown in Figure 27 might not be considered an appropriately 'conservative' idealisation for use in design. However, in practice such profiles are generally fitted (conservatively) through a number of CPT profiles, rather than being a strict lower bound to all profiles. The purpose here is to explore what potential over prediction of capacity might arise from the mismatch of the shear strength profiles in the upper few metres.

For the shallow foundation systems considered by Schneider et al. (2018), the vertical capacity of strip foundations of widths 5 to 20 m estimated using the CPT data directly were some 15% lower than those based on the idealised s_u profile. More significant differences were found for a foundation system compromising two linked skirted foundations, with skirt tips embedded 1.75 m, where the moment capacity using the CPT data was less than 50% of that from the idealised profile.

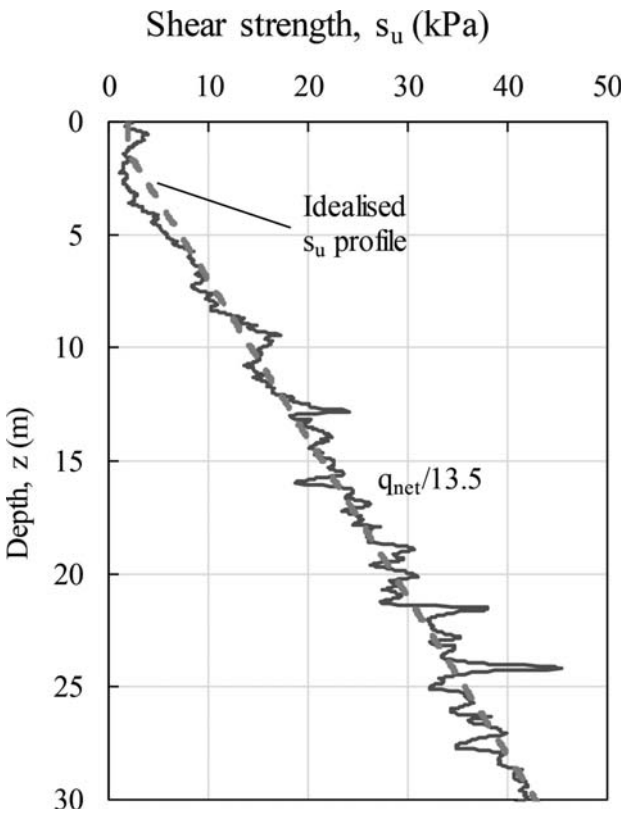

Figure 27. Strength profiles from Schneider et al. (2018).

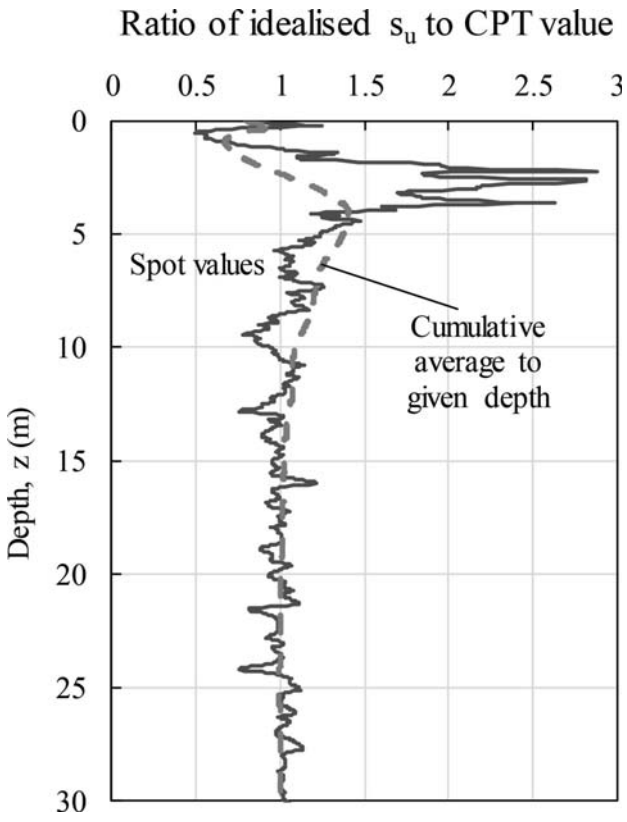

Figure 28. Ratios of spot values and cumulative averages for the idealised and 'direct' s_u profiles.

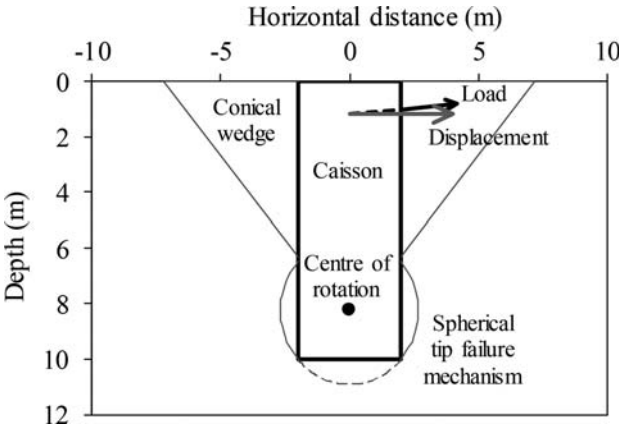

Figure 29. Suction anchor and upper bound failure mechanism.

Table 1. Strength and anchor capacities for different s_u profiles.

	CPT data	Idealised s_u	Ratio
Average s_u (0 to 10 m)	6.7 kPa	7.3 kPa	0.92
Anchor capacity (rotating)	828 kN	957 kN	0.86
Anchor capacity (translating)	3041 kN	3278 kN	0.93

Considering the profiles of cumulative average strength ratio shown in Figure 28, it might be expected that the capacity of a suction anchor would be relatively insensitive to the detailed stratigraphy observed from the CPT data, in particular the weak zone between 2 and 5 m depth. However, there are still significant differences.

Common applications for suction anchors for deep water developments include relatively small caissons for manifolds and pipeline end terminations. Typically, lateral loading for such caissons is applied near the seabed surface, leading to a rotational failure mode.

Figure 29 shows a 4 m diameter caisson embedded to a depth of 10 m, with loading applied at a depth of 1 m at an angle of 5 ° from the horizontal. The corresponding upper bound failure mechanism (Murff & Hamilton 1993) is as indicated, with a conical wedge failure extending to a depth of about 6 m, below which there is a rotating spherical failure.

Upper bound capacities evaluated using either the factored CPT data directly or the linearised s_u profile shown in Figure 27 are 828 kN and 957 kN respectively. The nearly 15% difference may be attributed partly to the approximately 9% difference in the cumulative average shear strength for the two profiles between 0 and 10 m. However, the weaker upper soil layer leads to further difference in capacity for a caisson with loading applied near the ground surface. By contrast, capacities for a purely horizontally translating caisson differ by just the difference in average shear strength over the relevant depth range. These results are summarised in Table 1.

It is possible to obtain similar capacities by judicious choice of the idealised s_u profile (for example, a crustal shear strength of 2.1 kPa, below which the shear strength is given by $s_u = -4.2 + 2z$ kPa). However, offshore design tends to follow a phased approach, with a geotechnical interpretive report providing simplified strength profiles for a range of possible foundation or anchoring systems, and detailed design undertaken in a subsequent engineering phase. The potential for significant overestimation of capacities due to subtle limitations in the idealised strength profiles is evident.

6 SUMMARY

This paper has considered a number of issues pertaining to penetrometer testing and interpretation with respect to offshore geotechnical design. The important trends are for improved cost-effectiveness, timely acquisition of quantitative strength (or

other design) data, and increased sophistication in testing and control procedures.

In keeping with these trends, the paper has included extended discussion of free-fall penetrometers and the techniques required to obtain equivalent 'static' strength or resistance parameters. Similarly, the potential for integrating box core sampling and deck-based penetrometer testing in early phases of (geophysical focused) site investigation has been discussed. The manner of the box-core tests, with close control of load and displacement on different axes of motion, is extendable to seabed-based testing, consistent with the underlying objective of 'bringing the laboratory to the seabed'.

A final consideration has been the manner in which penetrometer data should be utilised in design calculations. Important issues here are (a) to make appropriate allowances for the differences in scale between penetrometers, seabed layering and the design target; and (b) the increasing potential to incorporate the full detail of CPT data in design calculations.

ACKNOWLEDGEMENTS

This work forms part of the activities of the Centre for Offshore Foundation Systems at UWA, currently supported as a node of the Australian Research Council Centre of Excellence for Geotechnical Science and Engineering. The authors are grateful for support from the RIGSS JIP sponsors: Fugro, Shell, Total and Woodside Energy. In addition, Mark Randolph acknowledges support through the Fugro Chair in Geotechnics and David White acknowledges support through the Shell Chair in Offshore Engineering.

REFERENCES

Amodio, A., Erbrich, C.T., Murugavel, V. & Moyle, I. 2015. Re-visiting Yolla—managing jack-up storm stability: geotechnical assessment. *Proc. 15th Int. Conf. The Jack-Up Platform Design, Construction & Operation*, London.

API 2011. *RP 2GEO—Geotechnical and foundation design considerations.* American Petroleum Institute, Washington.

Aubeny, C.P. & Shi, H. 2006. Interpretation of impact penetration measurements in soft clays. *J. Geotech. & Geoenv. Eng.*, ASCE, 132(6): 770–777.

Beard, R.M., 1985. Expendable Doppler penetrometer for deep ocean sediment measurements. *ASTM Special Technical Publication*, 883: 101–124.

Been, K., Jefferies, M.G., & Hachey, J. 1991. The critical state of sands. *Géotechnique*, 41(3): 365–381.

Bienen, B., Cassidy, M.J., Randolph, M.F. & Teh, K.L. 2010. Characterisation of undrained shear strength using statistical methods. *Proc. 2nd Int. Symp. Frontiers in Offshore Geotech. ISFOG2010*, Taylor & Francis, London: 661–666.

Bienen, B., Pucker, T. & Henke, S. 2012. Cone penetrometer based spudcan penetration prediction in uncemented carbonate sand. *Proc. Offshore Technology Conf.*, Houston, Paper OTC 23002.

Bienen, B., Qiu, G. & Pucker, T. 2015. CPT correlation developed from numerical analysis to predict jack-up foundation penetration into sand overlying clay. *Ocean Engineering*, 108: 216–226.

Biscontin, G. & Pestana, J.M. 2001. Influence of peripheral velocity on vane shear strength of an artificial clay. *Geotechnical Testing Journal*, 24(4): 423–429.

Blake, A., O'Loughlin, C.D., Morton, J., O'Beirne, C., Gaudin, C. & White, D.J. 2016. In-situ measurement of the dynamic penetration of free-fall projectiles in soft soils using a low cost inertial measurement unit. *Geotechnical Testing Journal*, 39(2): 235–251.

Bolton, M.D., 1986. The strength and dilatancy of sands. *Géotechnique*, 36(1): 65–78.

Boscardin, A.G. & DeGroot, D.J. 2015. Evaluation of a toroid for model pipeline testing of very soft offshore box core samples. *Proc. 3rd Int. Symp. Frontiers in Offshore Geotech. ISFOG2015*, Taylor & Francis, London: 363–368.

Chow, S.H. & Airey, D.W. 2014. Free-falling penetrometers: a laboratory investigation in clay. *J. Geotech. & Geoenv. Eng.*, ASCE, 140(1): 201–214.

Chow, S.H., Bienen, B. & Randolph, M.F. 2018. Rapid penetration of piezocones in sand. *Proc. Int. Symp. Cone Penetration Testing, CPT'18*, Delft.

Chow, S.H., O'Loughlin, C.D. & Randolph, M.F. 2014. Soil strength estimation and pore pressure dissipation for free-fall piezocone in soft clay. *Géotechnique*, 64(10): 817–827.

Chow, S.H., O'Loughlin, C.D., White, D.J. & Randolph, M.F. 2017. An extended interpretation of the free-fall piezocone test in clay. *Géotechnique*, *67*(12): 1090–1103.

Clukey, E.C., Aubeny, C., Zakeri, A., Randolph, M.F., Sharma, P.P., White, D.J., Sancio, R. & Cerkovnik, M. 2017. A perspective on the state of knowledge regarding soil-pipe interaction for SCR fatigue assessments. *Proc. Offshore Technology Conf.*, Houston, Paper OTC 27564.

DNVGL 2017. *Pipe-soil interaction for submarine pipelines. Recommended Practice F-114,* DNVGL, Oslo.

Edwards, D., Bienen, B., Pucker, T. & Henke, S. 2013. Evaluation of the performance of a CPT-based correlation to predict spudcan penetrations using field data. *Proc. 14th Int. Conf. The Jack-Up Platform—Design, Design, Construction & Operation*, London.

Erbrich, C.T. 2005. Australian frontiers—spudcans on the edge. *Proc. Int. Symp. on Frontiers in Offshore Geotechnics, ISFOG*, Perth: 49–74.

Erbrich, C.T., Amodio, A., Krisdani, H., Lam S.Y., Xu, X. & Tho, K.K. 2015. Re-visiting Yolla—new insights on spudcan penetration. *Proc. 15th Int. Conf. The Jack-Up Platform Design, Construction & Operation*, London.

Fawaz, A., Teoh, A., Airey, D.W. & Hubble, T. 2016. Soil strength in the Murray River determined from a free falling penetrometer. Proc. *5th Int. Conf. on Geo-*

tech. & Geophysical Site Characterisation, ISC'5 Gold Coast: 1217–1222.

Furlong, A., Osler, J.C., Christian, H., Cunningham, D. & Pecknold, S. 2006. The moving vessel profiler (MVP) - a rapid environmental assessment tool for the collection of water column profiles and sediment classification. *Proc. Undersea Defence Technology Pacific Conf.*, San Diego: 1–13.

Geirnaert, K., Staelens, P., Deprez, S., Noordijk, A. & Van Hassent, A. 2013. Innovative free fall sediment profiler for preparing and evaluating dredging works and determining the nautical depth. *WODCON XX*: 1–11.

Hunt, R., 2008. Achieving operational excellence for jack-up rig deployments—how shall we get there? *Proc. 2nd Jack-Up Asia Conf. and Exhibition*, Singapore.

ISO, 2012. *Petroleum and natural gas industries—site-specific assessment of mobile offshore units—part 1: Jack-ups, 19905–1,* Int. Organization for Standardization, Geneva.

Jack, R.L., Hoyle, M.J.R., Smith, N.P. & Hunt, R.J. 2013. Jack-up accident statistics—a further update. *Proc. 14th Int. Conf. The Jack-Up Platform—Design, Const. & Oper.*, London.

Kelleher, P., Low, H.E., Jones, C., Lunne, T., Strandvik, S. & Tjelta, T.I. 2011. Strength measurement in very soft upper seabed sediments. *Proc. 2nd Int. Symp. Frontiers in Offshore Geotech. ISFOG2010*, Taylor & Francis, London: 283–288.

Kopf, A., Stegmann, S., Krastel, S., Foerster, A., Strasser, M. & Irving, M. 2007. Marine deep-water free-fall CPT measurements for landslide characterisation off Crete, Greece (Eastern Mediterranean Sea), part 2: initial data from the western Cretan Sea. *Proc. Int. Conf. Submarine Mass Movements and Their Consequences*. Springer, Netherlands: 199–208.

Lee, J. & Randolph, M.F. 2011. Penetrometer-based assessment of spudcan penetration resistance. *J. Geotech. & Geoenv. Eng.*, ASCE, 137(6): 587–596.

Lehane, B.M., O'Loughlin, C.D., Gaudin, C., & Randolph, M.F. 2009. Rate effects on penetrometer resistance in kaolin. *Géotechnique*, 59(1), 41–52.

Low, H.E., Randolph, M.F., Rutherford, C.J., Bernard, B.B. & Brooks, J.M. 2008. Characterization of near seabed surface sediment. *Proc. Offshore Technology Conf.*, Houston, Paper OTC 19149.

Lucking, G., Stark, N., Lippmann, T. & Smyth, S. 2017. Variability of in situ sediment strength and pore pressure behavior of tidal estuary surface sediments, *Geo-Marine Letters*, 37(5): 441–456.

Mahmoodzadeh, H., Wang, D. & Randolph, M.F. 2015. Interpretation of piezoball dissipation testing in clay. *Géotechnique*, 65(10): 831–842.

Morton, J.P., O'Loughlin, C.D. & White, D.J. 2016a. Estimation of soil strength in fine-grained soils by instrumented free-fall sphere tests. *Géotechnique*, 66(12): 959–968.

Morton, J.P., O'Loughlin, C.D. & White, D.J. 2016b. Centrifuge modelling of an instrumented free-fall sphere for measurement of undrained strength in fine-grained soils. *Canadian Geotech. J.*, 53: 918–929.

Mosher, D.C., Christian, H., Cunningham, D., Mackillop, K., Furlong, A., & Jarrett, K. 2007. The Harpoon Free Fall Cone Penetrometer for Rapid Offshore Geotechnical Assessment. *Proc. 6th Int. Offshore Site Investigation and Geotechnics Conf.*, London: 195–202.

Mulhearn, P.J. 2003. Influences of penetrometer tip geometry on bearing strength estimates. *Int. J. of Offshore and Polar Eng.*, 13(1): 73–78.

Mumtaz, M.B., Stark, N. & Brizzolara, S. 2018. Pore pressure measurements using a portable free fall penetrometer. *Proc. Int. Symp. Cone Penetration Testing, CPT'18*, Delft.

Murff, J.D. & Hamilton, J.M. 1993. P-ultimate for undrained analysis of laterally loaded piles, *J. Geotechnical Eng.*, ASCE, 119 (1): 91–107.

O'Beirne, C., O'Loughlin, C.D. & Gaudin, C. 2017. A release-to-rest model for dynamically installed anchors, *J. Geotech. & Geoenv. Eng.*, ASCE, 143(9): 04017052.

O'Loughlin, C.D., Blake, A.P. & Gaudin, C. 2016. Towards a design method for dynamically embedded plate anchors, *Géotechnique*, 66(9): 741–753.

O'Loughlin, C.D., Gaudin, C., Morton, J.P. & White, D.J. 2014. MEMS accelerometers for measuring dynamic penetration events in geotechnical centrifuge tests. *Int. J. Physical Modelling in Geotech.*, 14(2): 31–39.

O'Loughlin, C.D., Randolph, M.F. & Richardson, M.D. 2004. Experimental and theoretical studies of deep penetrating anchors. *Proc. Offshore Tech. Conf.*, Houston, OTC 16841.

O'Loughlin, C.D., Richardson, M.D., Randolph, M.F. & Gaudin, C. 2013. Penetration of dynamically installed anchors in clay. *Géotechnique*, 63(11): 909–919.

Orenberg, P., True, D.G., Bowman, L., Herrmann, H. & March, R. 1996. Use of a dropped dynamic penetrometer in cohesionless soil. *Proc. Offshore Tech. Conf.*, Houston, Paper OTC 8027.

Osborne, J.J., Pelley, D., Nelson, C. & Hunt, R. 2006. Unpredicted jack-up foundation performance. *Proc. Jack-Up Asia Conf. and Exhibition*, Singapore.

Osborne, J.J., Teh, K.L., Houlsby, G.T., Cassidy, M.J., Bienen, B. & Leung, C.F. 2011. *'InSafeJIP' – Improved Guidelines for the Prediction of Geotechnical Performance of Spudcan Foundations During Installation and Removal of Jack-up Units, Final Guidelines of the InSafe Joint Industry Project Report Number EOG0574-Rev1.* RPSEnergy, Woking, UK.

Peuchen, J., Looijen, P.N. & Stark, N. 2017. Offshore characterisation of extremely soft sediments by free fall penetrometer. *Proc. 8th Int. Conf. Offshore Site Investigation and Geotechnics*, Soc. for Underwater Tech., London, 1: 370–377.

Peuchen, J. & Westgate, Z. 2018. Defining geotechnical parameters for surface-laid subsea pipe-soil interaction. *Proc. Int. Symp. Cone Penetration Testing, CPT'18*, Delft.

Pucker, T., Bienen, B. & Henke, S. 2013. CPT based prediction of foundation penetration in siliceous sand. *Applied Ocean Research*, 41: 9–18.

Randolph, M.F. 2016. New tools and directions in offshore site investigation—ISC'5 Keynote Lecture. *Australian Geomechanics*, 51(4): 81–92.

Randolph, M.F., Low, H.E. & Zhou, H. 2007. In situ testing for design of pipeline and anchoring systems. Keynote paper, *Proc. 6th Int. Conf. Offshore Site Investigation and Geotechnics*, Society for Underwater Technology, London: 251–262.

Robertson, P.K. 2016. Cone penetration test (CPT)-based soil behaviour type (SBT) classification system—an update. *Canadian Geotech. J*., 53(12): 1910–1927.

Robertson, P.K. & Wride, C.E. 1998. Evaluating cyclic liquefaction potential using the cone penetration test. *Canadian Geotech. J.*, 35(3): 442–459.

Rocker, K. 1985. *Handbook for marine geotechnical engineering*. Naval Civil Eng. Lab., Port Hueneme, CA.

Sabetamal, H., Carter, J.P., Nazem, M. & Sloan, S.W. 2016. Coupled analysis of dynamically penetrating anchors. *Computers & Geotechnics*, 77: 26–44.

Safinus, S. 2015. *Estimation of spudcan penetration resistance in stratified soils from field piezocone penetrometer data.* PhD Thesis, University of Western Australia.

Schneider, J.A., Doherty, J.P., Randolph, M.F. & Krabbenhoft, K. 2018. Direct use of CPT data for numerical analysis of VHM loading of shallow foundations. *Proc. Int. Symp. Cone Penetration Testing, CPT'18*, Delft.

Stanier, S. & White D.J. 2015. Shallow penetrometer penetration resistance. *J. Geotech. & Geoenv. Eng.*, ASCE, 141(3): 04014117.

Stark, N., Hanff, H. & Kopf, A.J. 2009. Nimrod: a tool for rapid geotechnical characterization of surface sediments. *Sea Technology*, 50(4): 10–14.

Stark, N., Hay, A.E. & Trowse, G. 2014. Cost-effective geotechnical and sedimentological early site assessment for ocean renewable energies. *2014 Oceans—St. John's*: 1–8.

Stark, N., Wilkens, R., Ernsten, V.B., Lambers-Huesman, M., Stegmann, S. & Kopf, A.J. 2012. Geotechnical properties of sandy seafloor and the consequences for dynamic penetrometer interpretations: quartz sand versus carbonate sand. *Geotechnical and Geological Engineering*, 30: 1–14.

Stegmann, S., Morz, T. & Kopf, A.J. 2006. Initial results of a new free fall-cone penetrometer (FF-CPT) for geotechnical in situ characterisation of soft marine sediments. *Norsk Geologisk Tidsskrift*, 86(3): 199–208.

Steiner, A., L'Heureux, J.S., Kopf, A., Vanneste, M., Longva, O., Lange, M. & Haflidason, H. 2012. An in-situ free-fall piezocone penetrometer for characterizing soft and sensitive clays at Finneidfjord (Northern Norway). *Proc. Int. Conf. Submarine Mass Movements and Their Consequences*. Adv. Natural & Tech. Hazards, 31, Springer: 99–109.

Steiner, A., Kopf, A.J., L'Heureux, J.S., Kreiter, S., Stegmann, S., Haflidason, H. & Moerz, T. 2014. In situ dynamic piezocone penetrometer tests in natural clayey soils–a reappraisal of strain-rate corrections. *Can. Geotech. J.*, 51(3): 272–288.

Stephan, S., Kaul, N. & Stark, N. 2011. LIRmeter: A new tool for rapid assessment of sea floor parameters. Bridging the gap between free-fall instruments and frame-based CPT. *Proc. MTS/IEEE OCEANS 2011*. IEEE *OCEANS*.

Stoll, R.D. & Akal, T. 1999. XBP-Tool for rapid assessment of seabed sediment properties. *Sea Technology*, 40(2): 47–51.

Thompson, D., March, R. & Herrmann, H. 2002. Groundtruth results for dynamic penetrometers in cohesive soils. In *Proceedings of OCEANS 2002, MTS/IEEE—Marine Frontiers: Reflection of the Past, Visions of the Future*, (4): 2117–2123.

True, D.G. 1976. *Undrained vertical penetration into ocean bottom soils.* PhD thesis, University of California, Berkeley.

White, D.J., Gaudin, C., Boylan, N. & Zhou, H. 2010. Interpretation of T-bar penetrometer tests at shallow embedment and in very soft soils. *Canadian Geotech. J.*, 47(2): 218–229.

White, D.J. & Randolph, M.F. 2007. Seabed characterisation and models for pipeline-soil interaction. *Int. J. Offshore & Polar Engng*., 17(3): 193–204.

White, D.J., O'Loughlin, C.D., Stark, N. & Chow, S.H. 2018. Free fall penetrometer tests in sand: Determining the equivalent drained resistance. *Proc. Int. Symp. Cone Penetration Testing, CPT'18*, Delft.

White, D.J., Stanier, S.A., Schneider, M.A., O'Loughlin, C.D., Chow, S.H., Randolph, M.F., Draper, S.D. Mohr, H, Morton, J.P., Peuchen, J., Fearon, R., Roux, A. & Chow, F.C. 2017. Remote intelligent geotechnical seabed surveys—technology emerging from the RIGSS JIP. *Proc. 8th Int. Conf. Offshore Site Investigation and Geotechnics*, Society for Underwater Technology, London, 2: 1214–1222.

White, D.J., Clukey, E.C., Randolph, M.F., Boylan, N.P., Bransby, M.F., Zakeri, A., Hill, A.J. & Jaeck, C. 2017. The state of knowledge of pipe-soil interaction for on-bottom pipeline design. *Proc. Offshore Tech. Conf.*, Houston, Paper OTC 27623.

Yan, Y., White D.J. & Randolph M.F. 2014. Cyclic consolidation and axial friction on seabed pipelines. *Géotechnique Letters*, 4: 165–169.

Yan Y., White D.J. & Randolph M.F. 2017. Elastoplastic consolidation solutions for scaling from shallow penetrometers to pipelines. *Canadian Geotech. J.*, 54: 881–895.

Yan Y. White D.J. & Randolph M.F. 2011. Penetration resistance and stiffness factors in uniform clay for hemispherical and toroidal penetrometers *Int. J. of Geomech.*, ASCE, 11: 263–275.

Young, A.G., Bernard, B.B., Remmes, B.D., Babb, L.V. & Brooks, J.M. 2011. "CPT Stinger"—an innovative method to obtain cpt data for integrated geoscience studies. *Proc. Offshore Tech. Conf.*, Houston, Paper OTC 21569.

Yuan, F., White, D.J. & O'Loughlin, C.D. 2017. The evolution of seabed stiffness during cyclic movement in a riser touchdown zone on soft clay. *Géotechnique*, 67(2): 127–137.